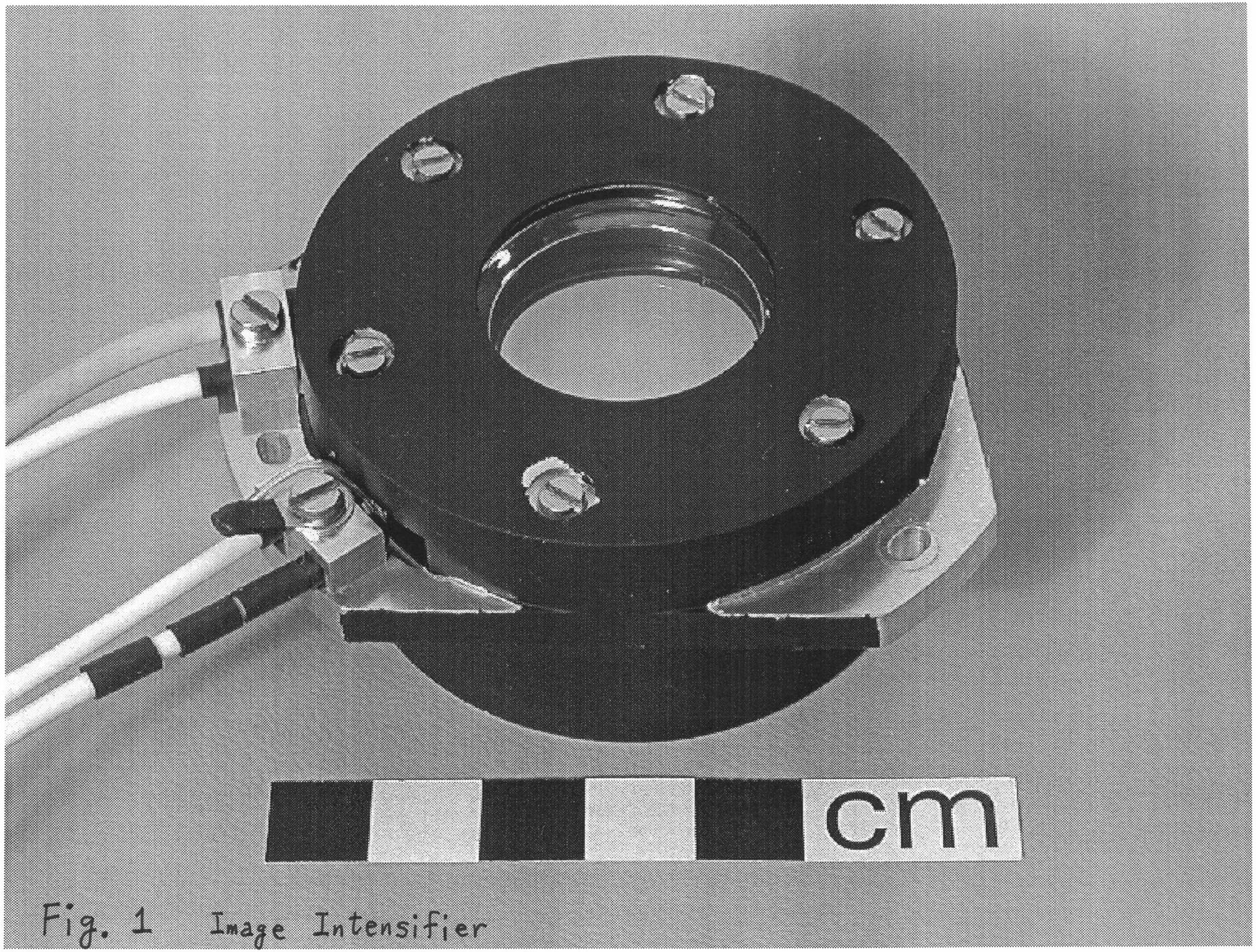

Fig. 1 Image Intensifier

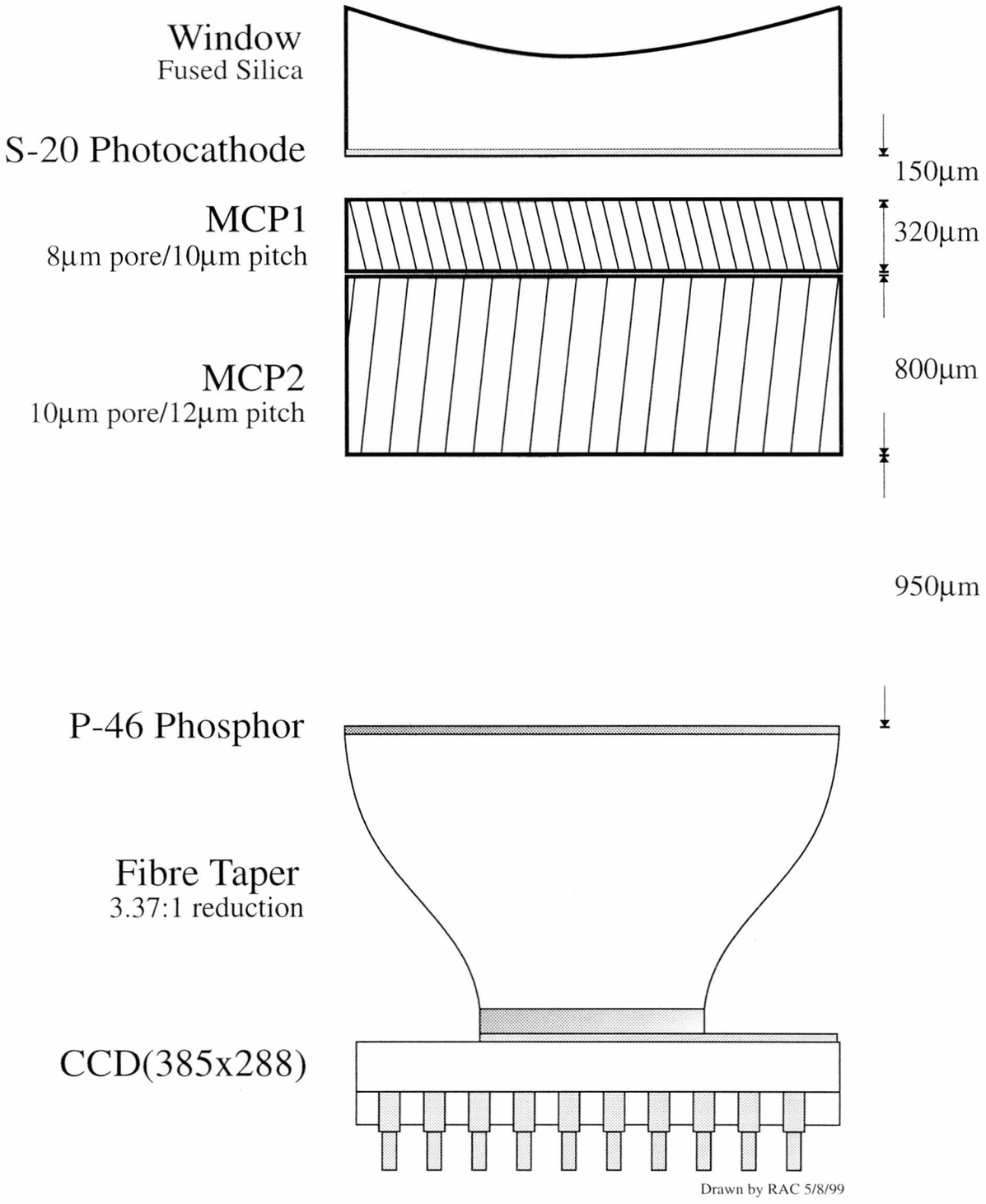

Fig.2 Schematic Structure of Detector Head

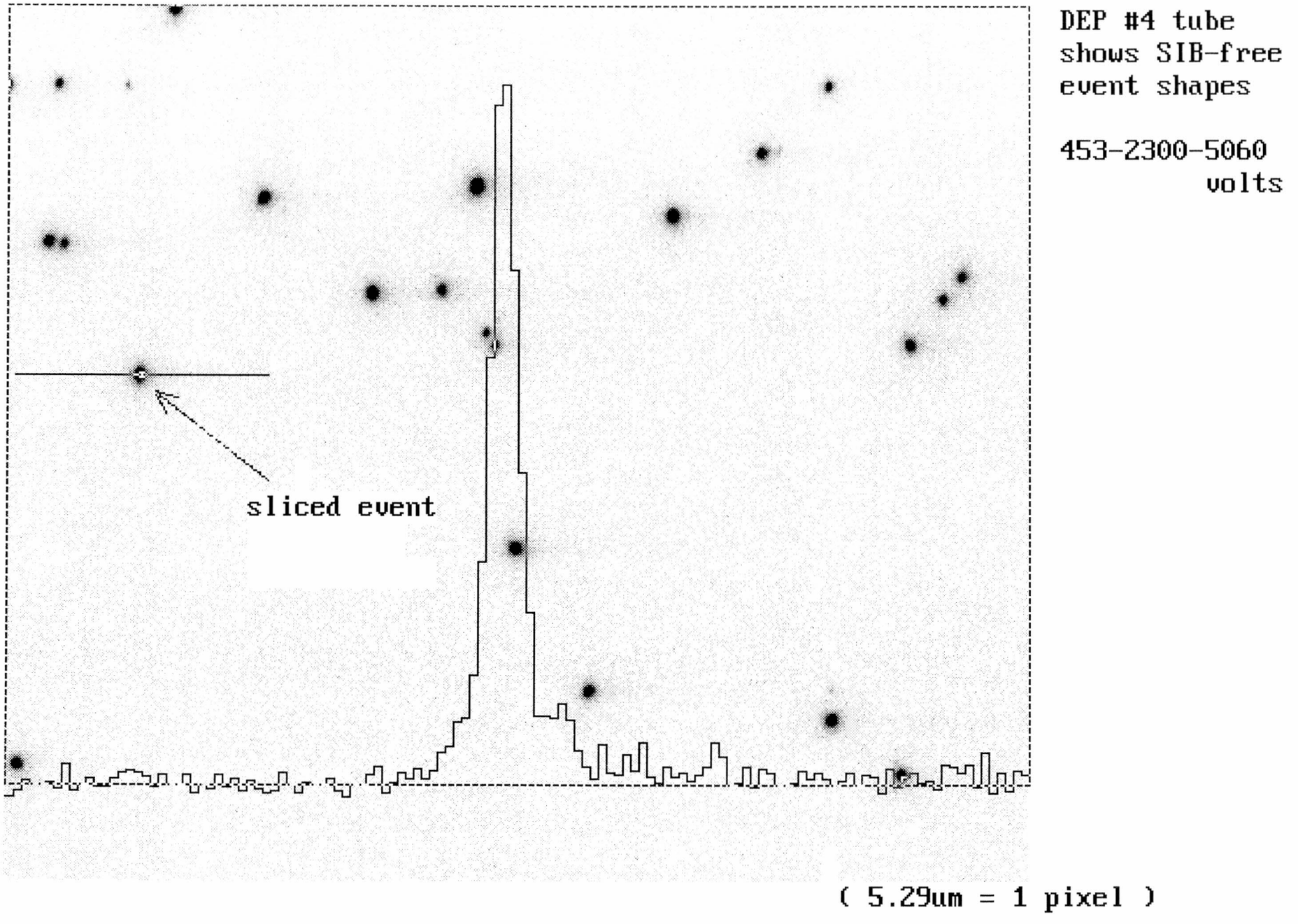

Fig. 3 Event profiles captured by a low noise CCD camera with x3 optics

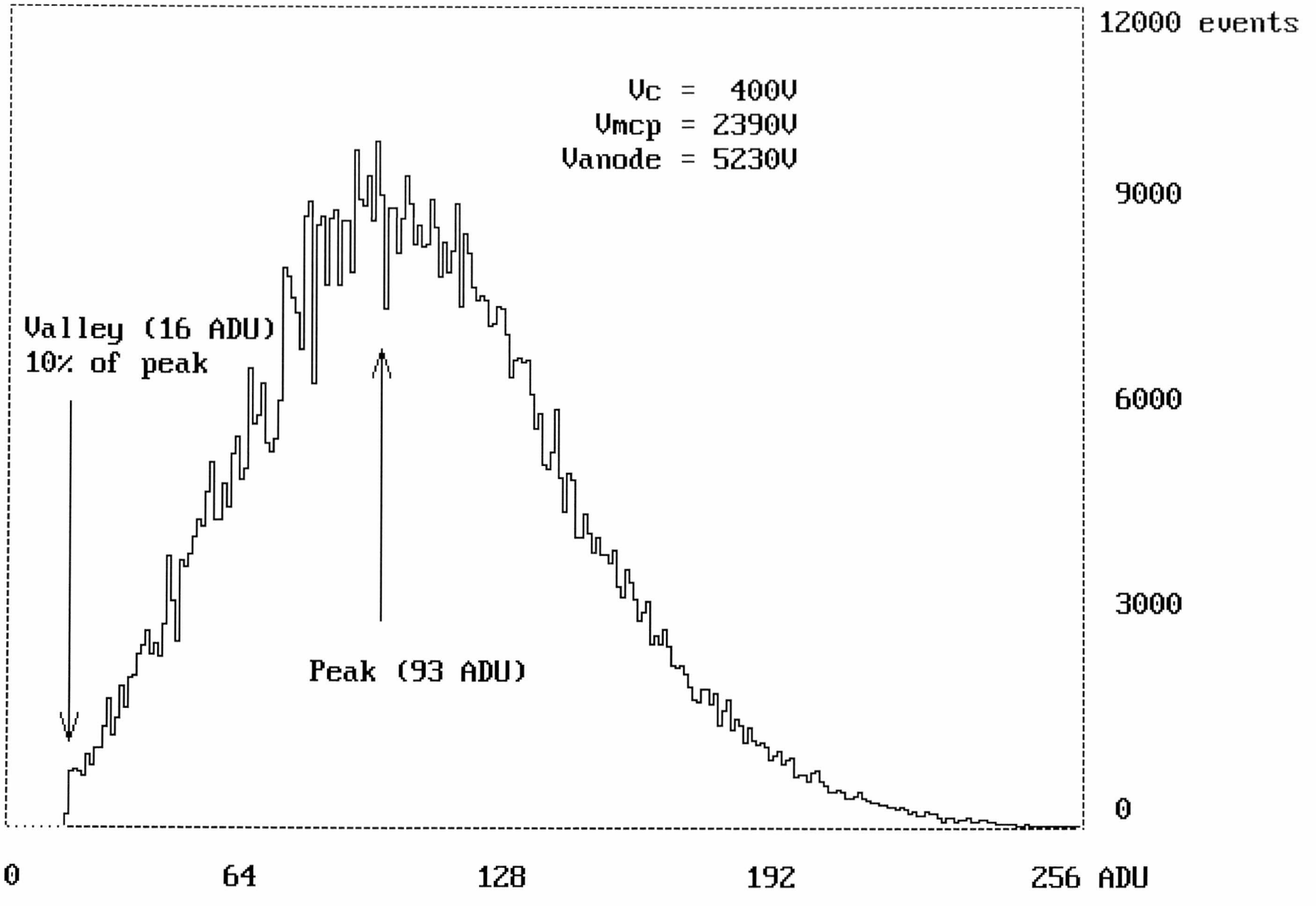

Fig. 4 Pulse height distribution of a XMM-OM FM-intensifer (DEP_#6)

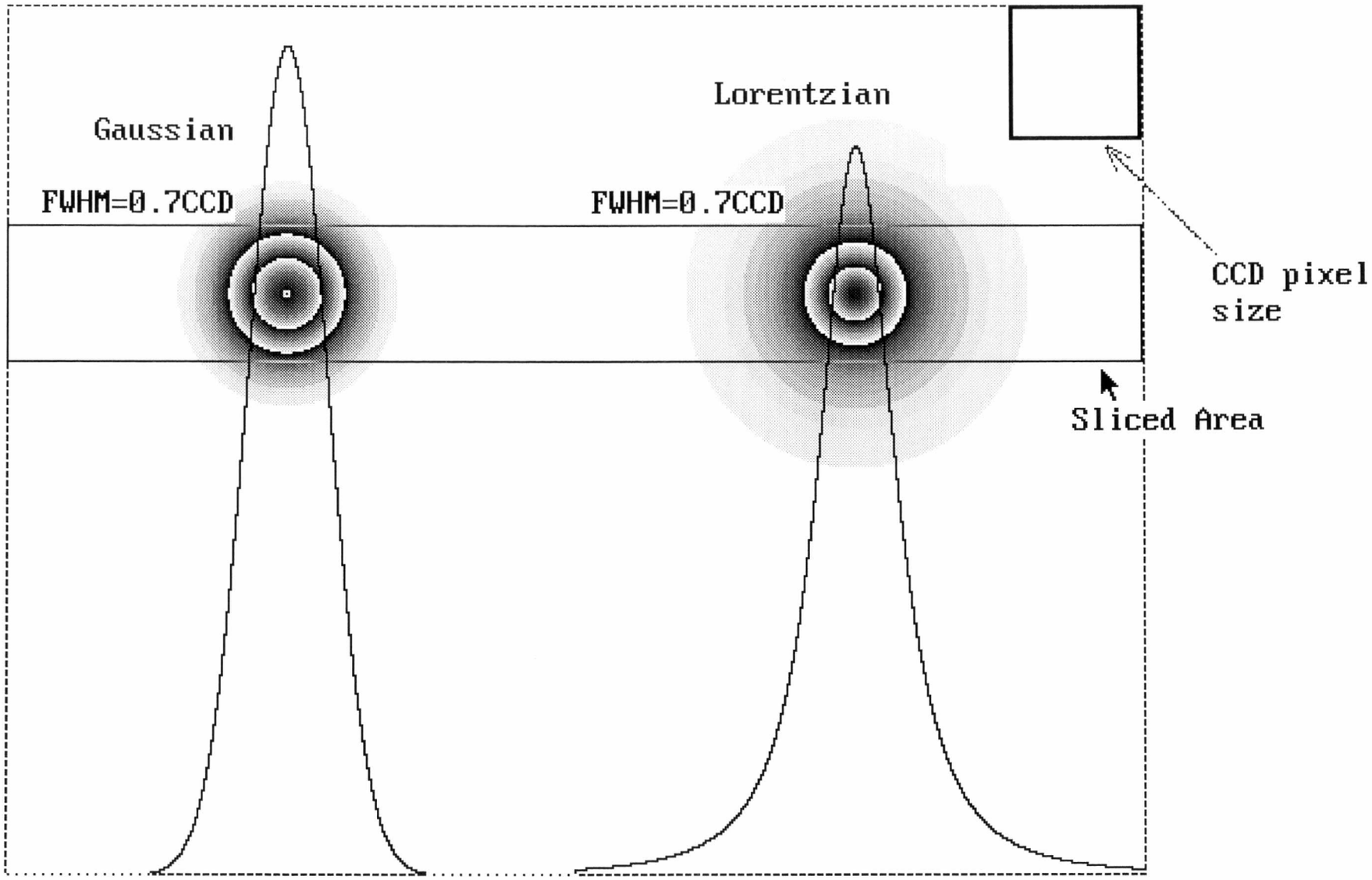

Fig. 5 Model event profiles

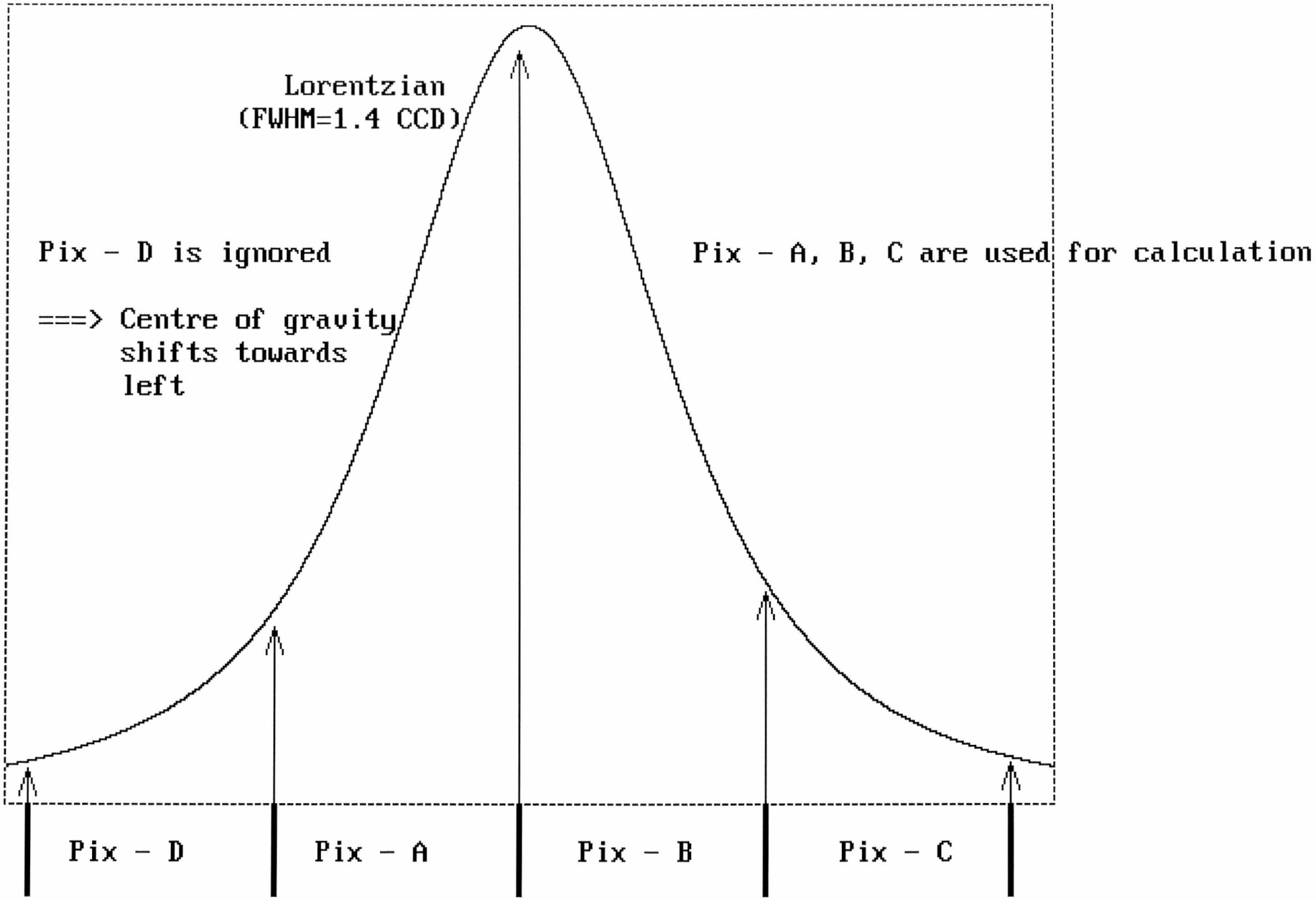

Fig. 6 Event capture by CCD pixels

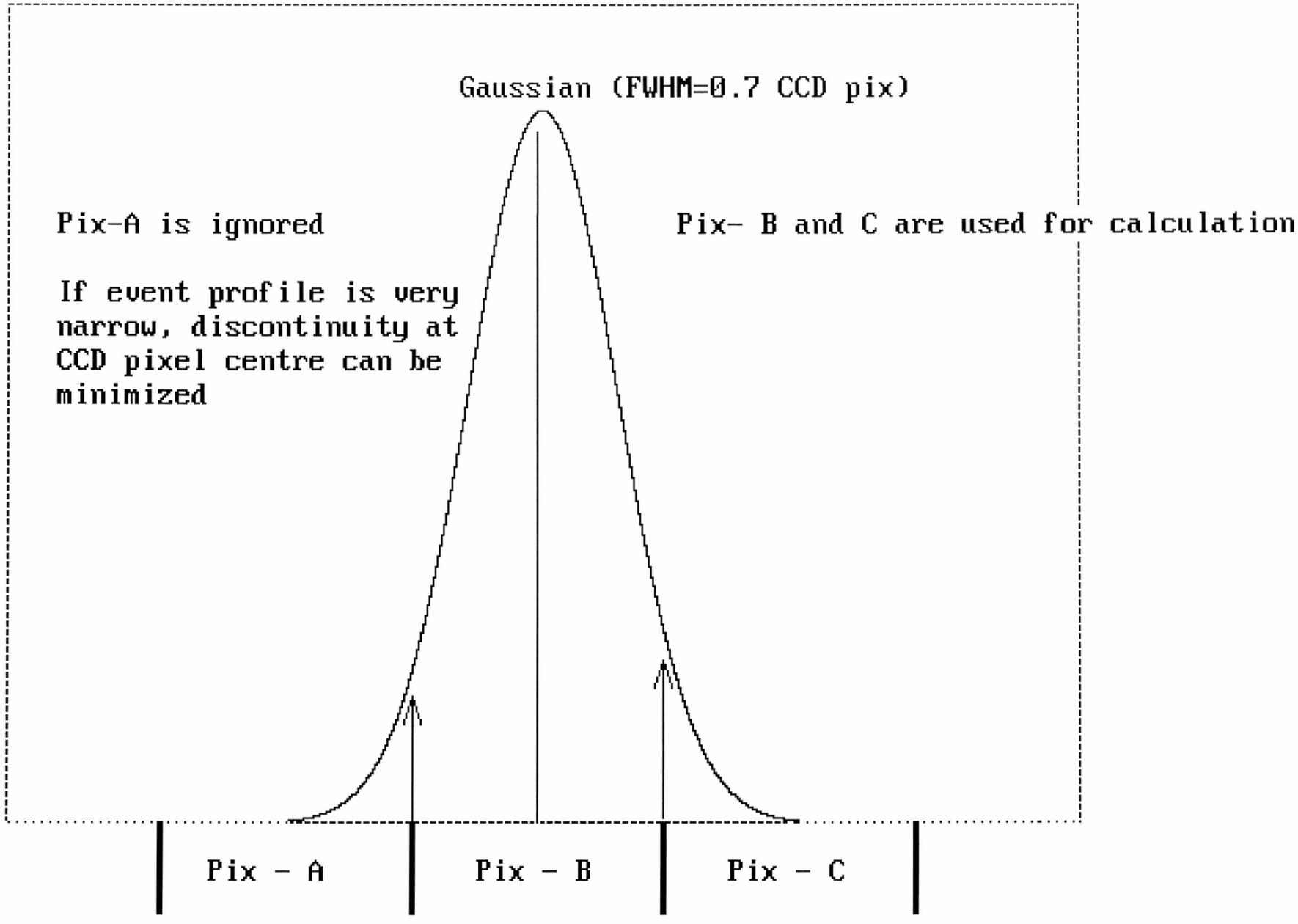

Fig. 7 Event capture by CCD pixels (2 pixels centre of gravity)

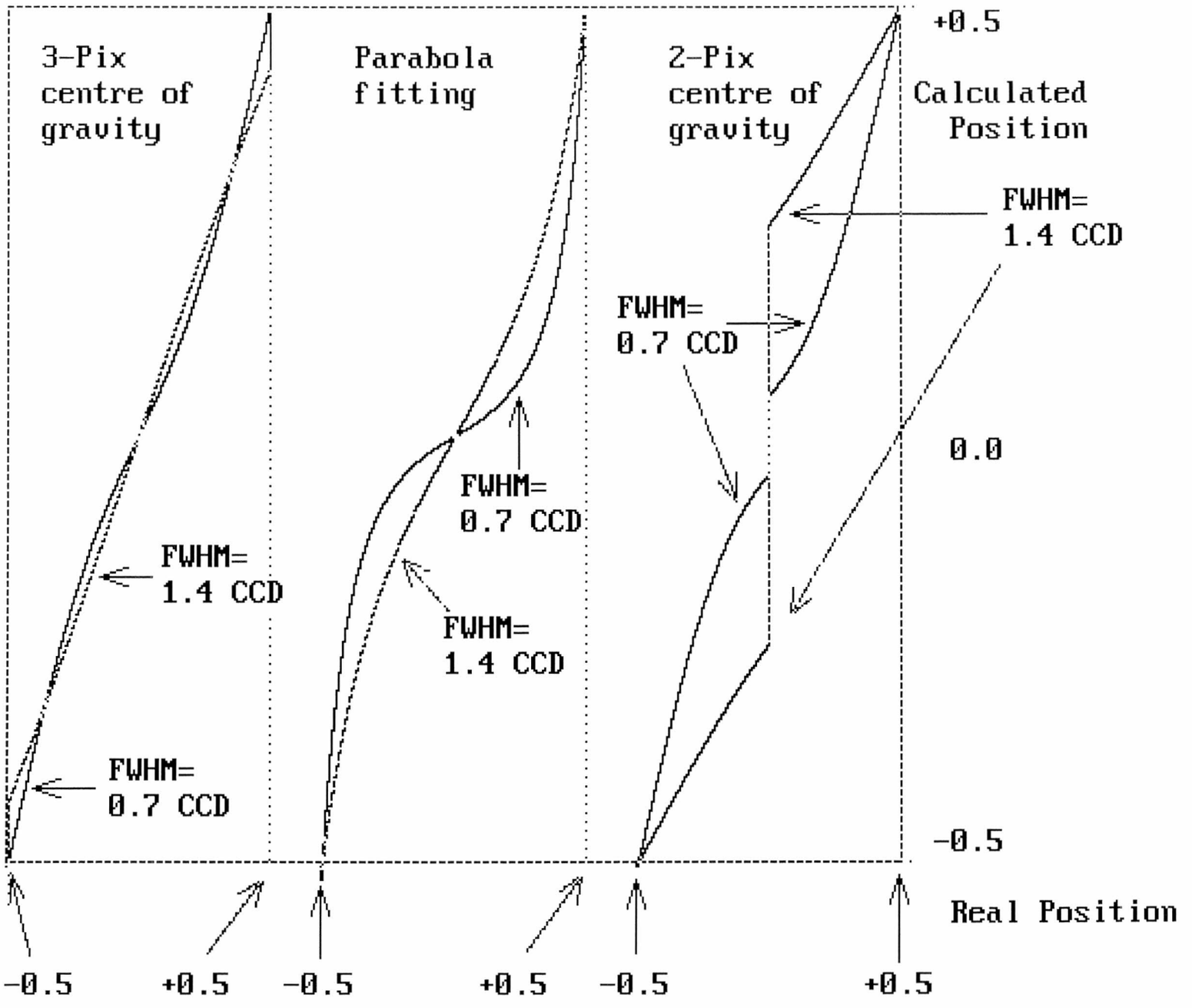

Fig. 8 Characteristic curves for 3 algorithms (Gaussian event profile)

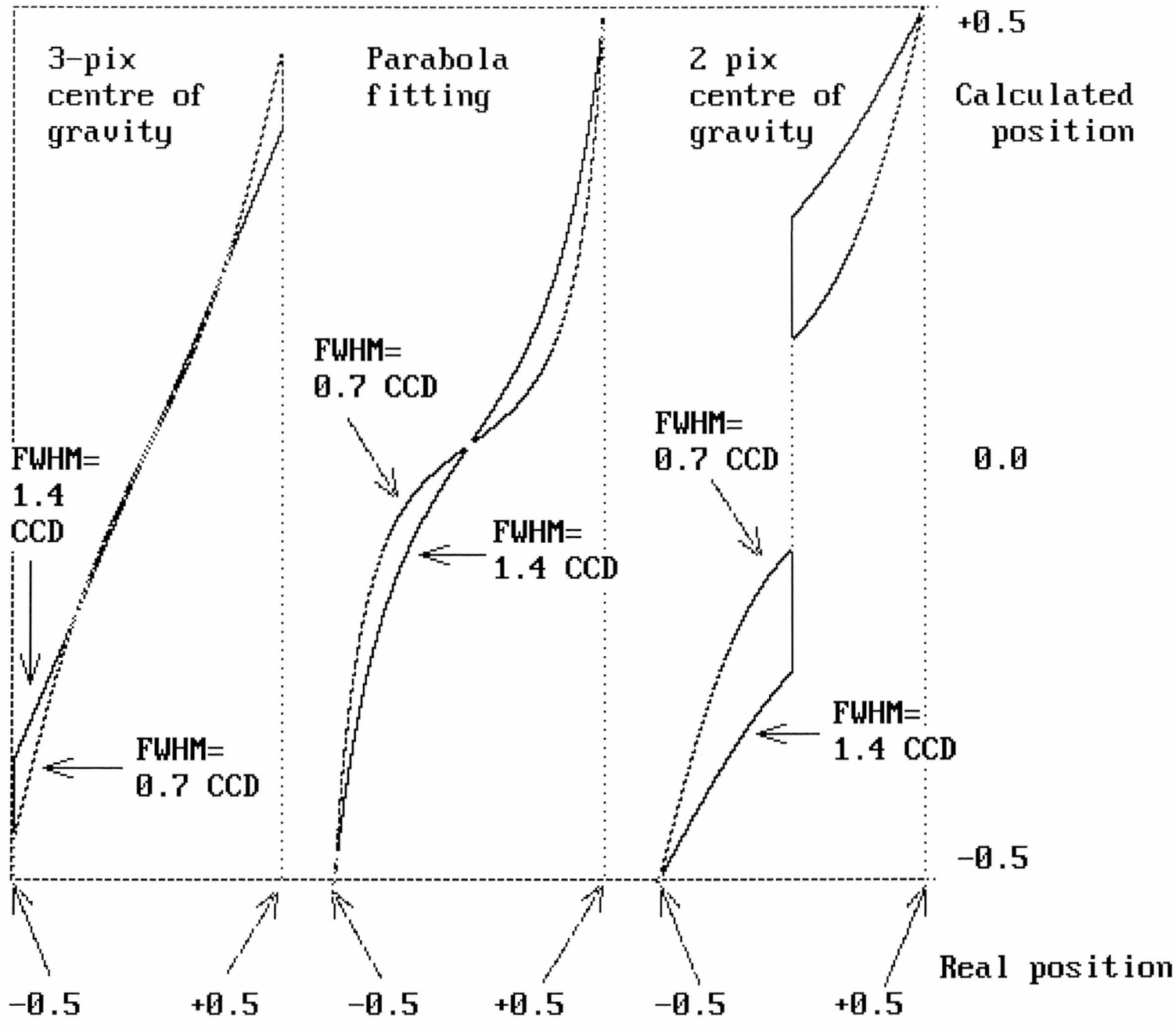

Fig. 9 Characteristic curves for 3 algorithms (Lorentzian event profile)

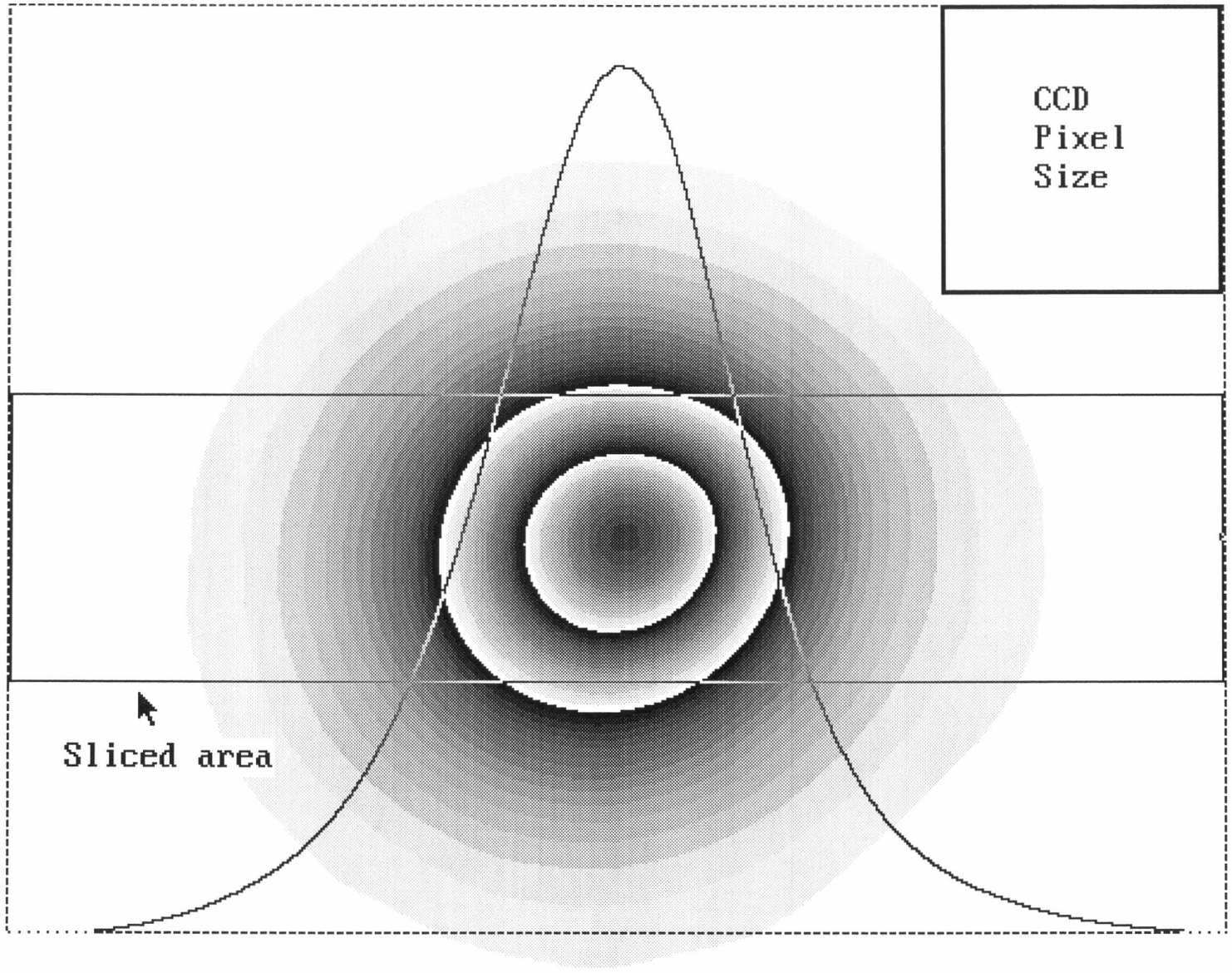

16H 15M 00S 16H 40M 00S 1999/09/22/

Fig. 10 Standard event profile of DEP_#8 intensifer 60 snap frames

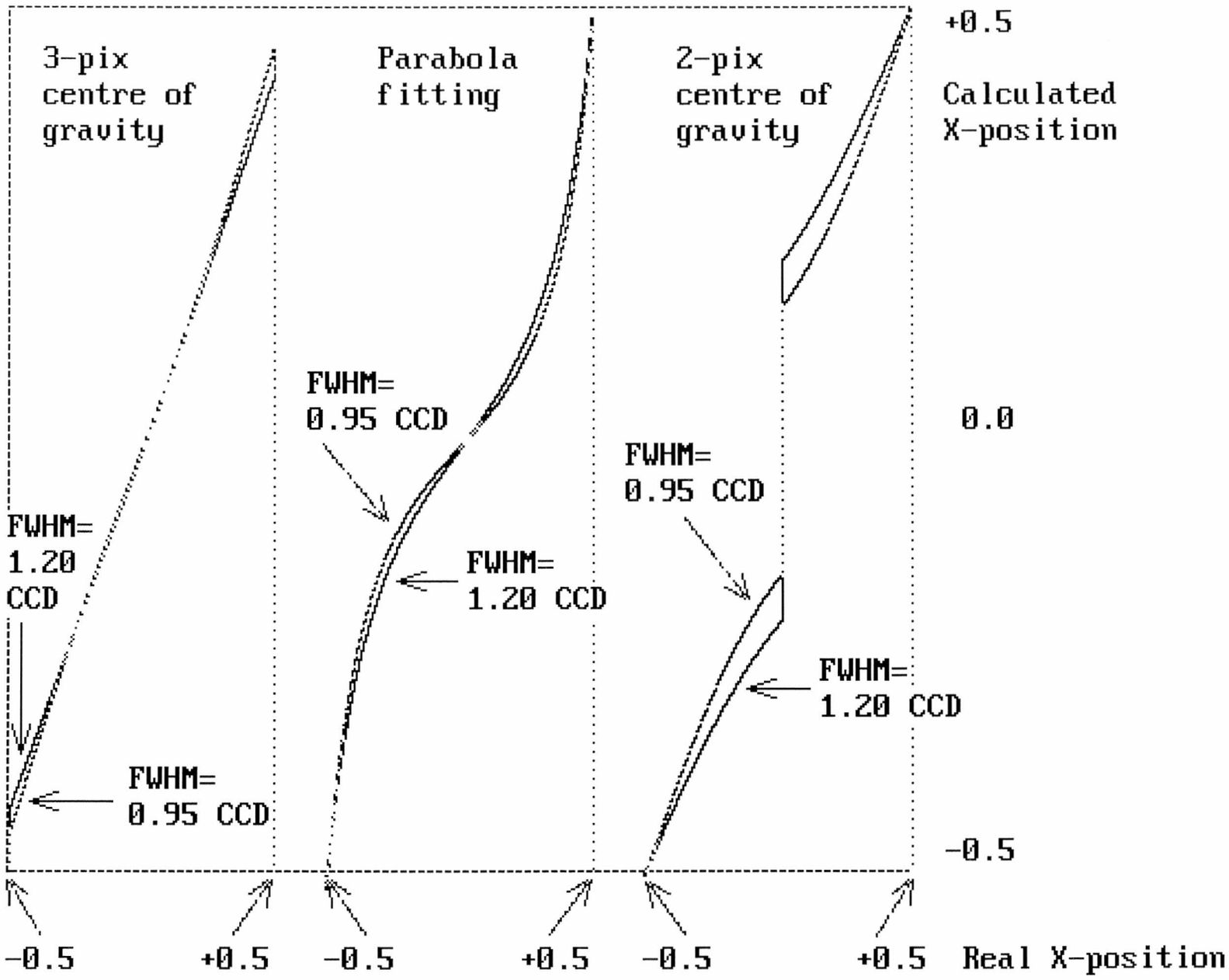

Fig. 11 Characteristic curves with true event profile slicing at Y-centre

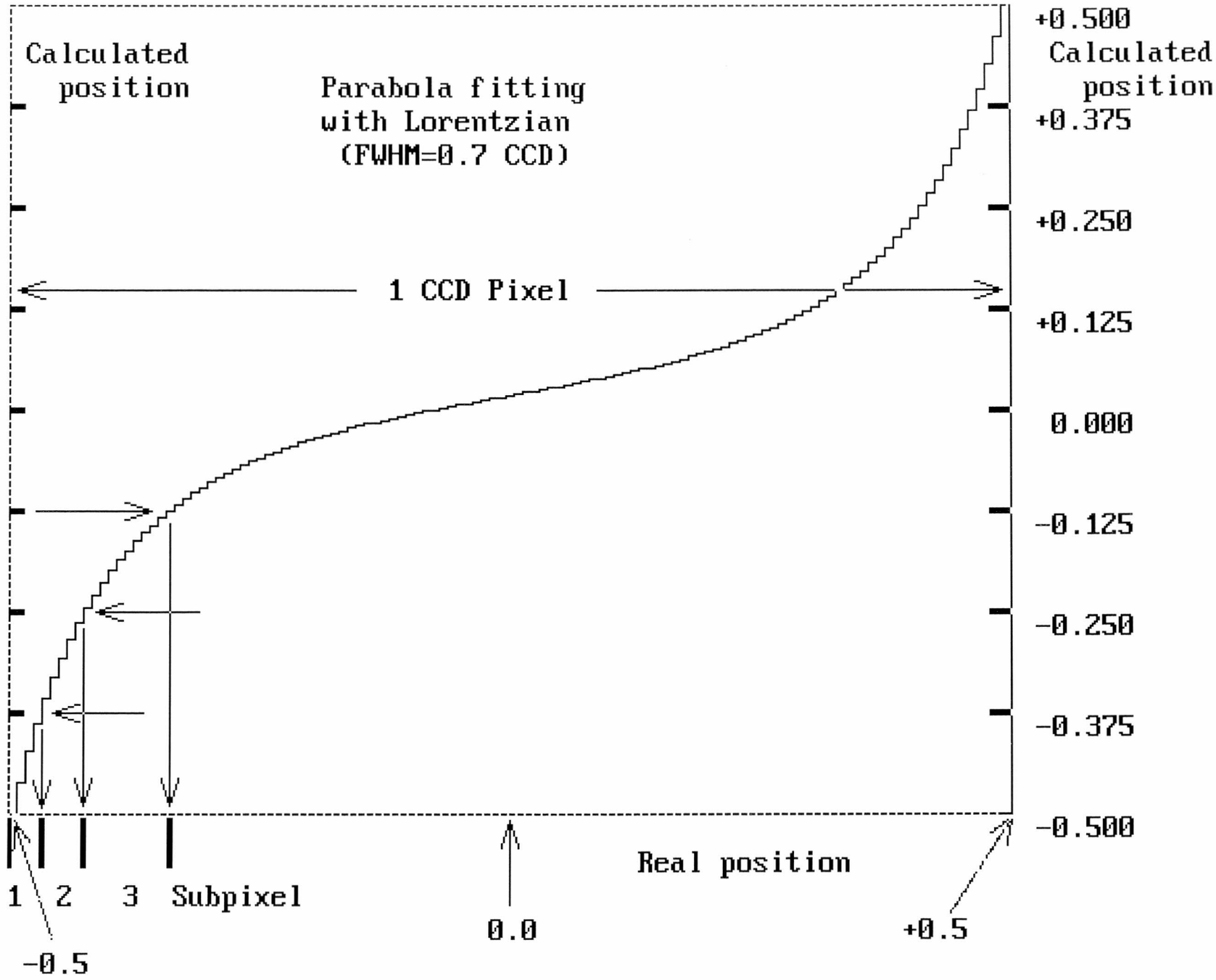

Fig. 12 Non-linear characteristic curve and Fixed pattern

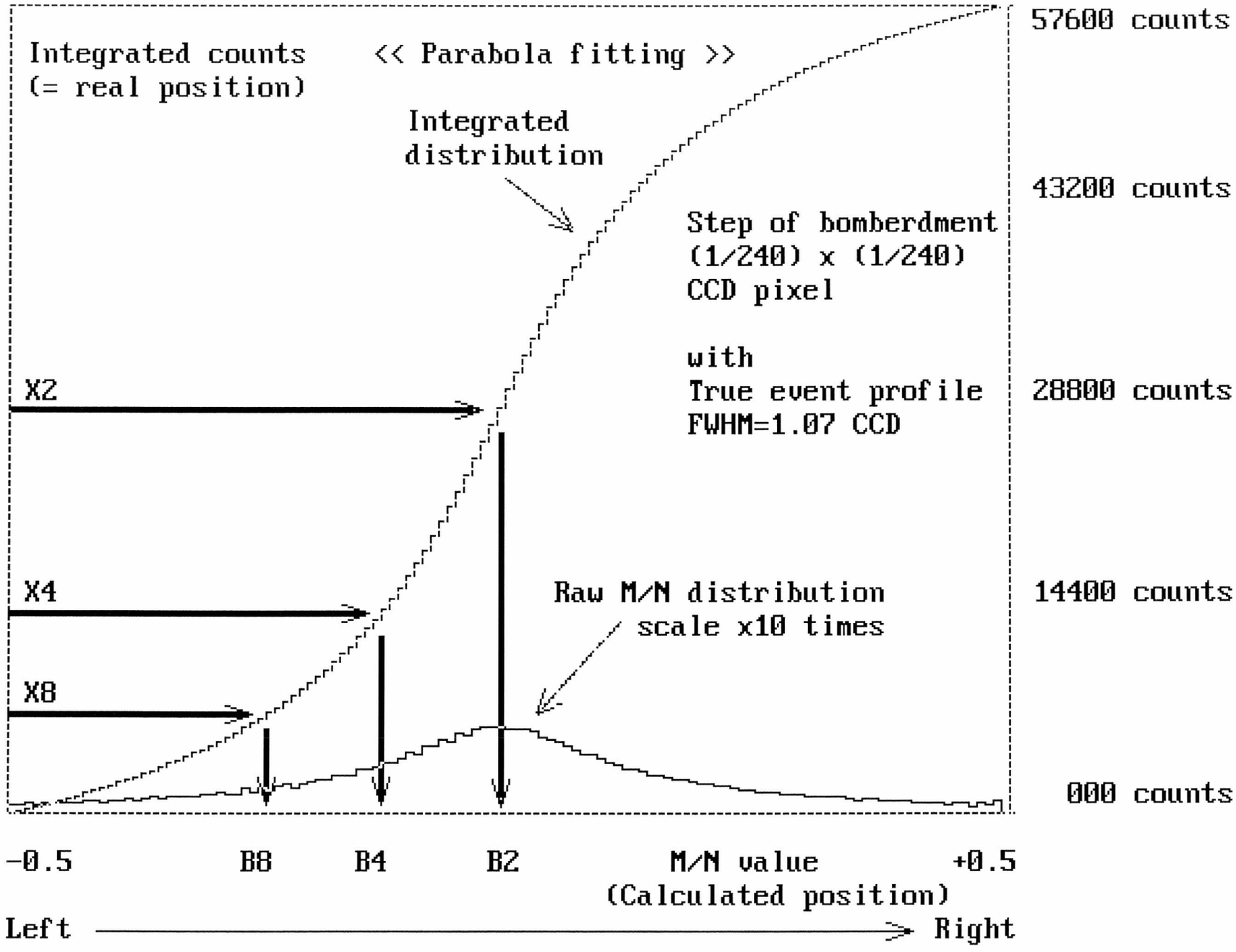

Fig. 13 M/N distribution by uniform bomberdment on a CCD pixel

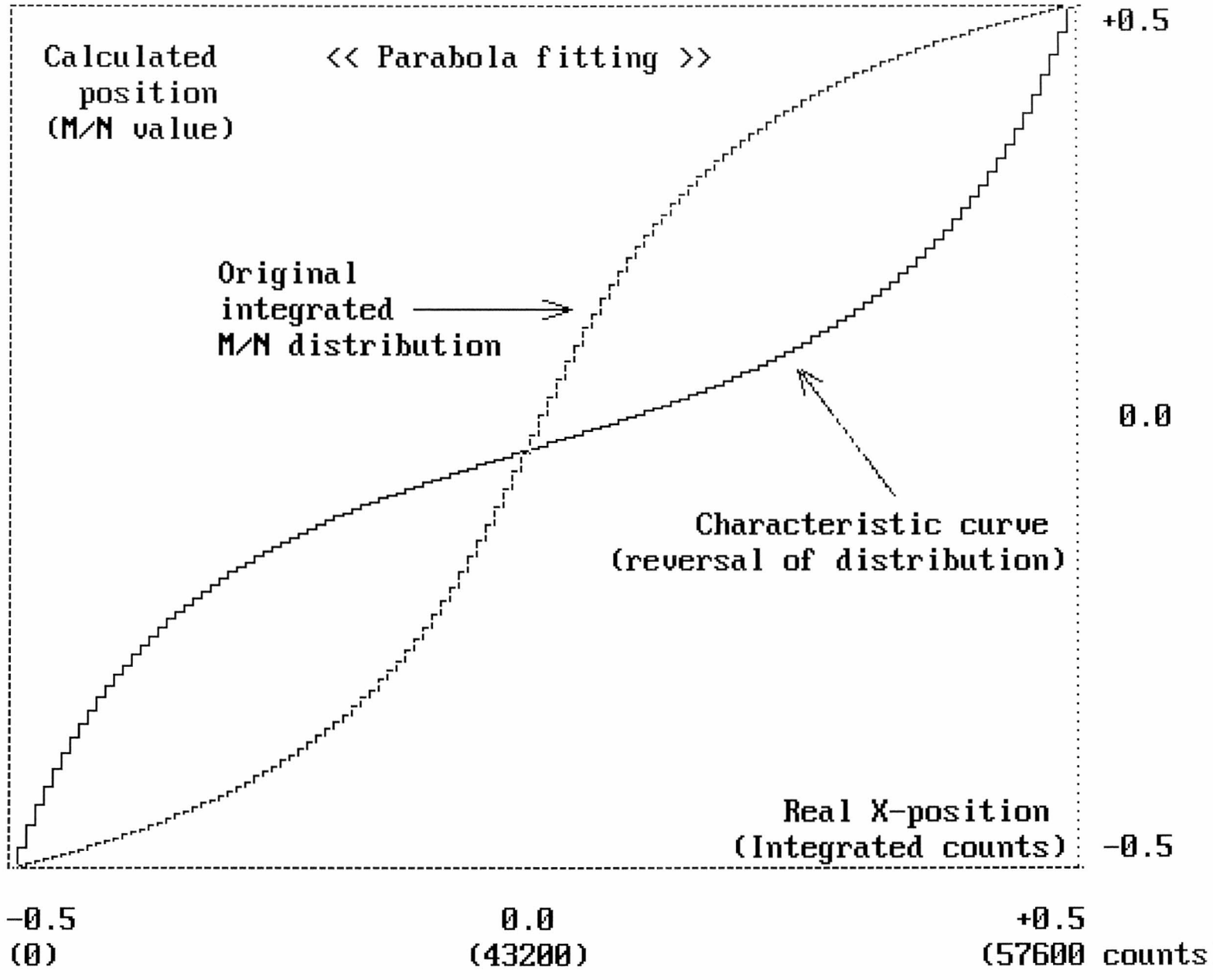

Fig. 14 Characteristic curve derived from M/N distribution

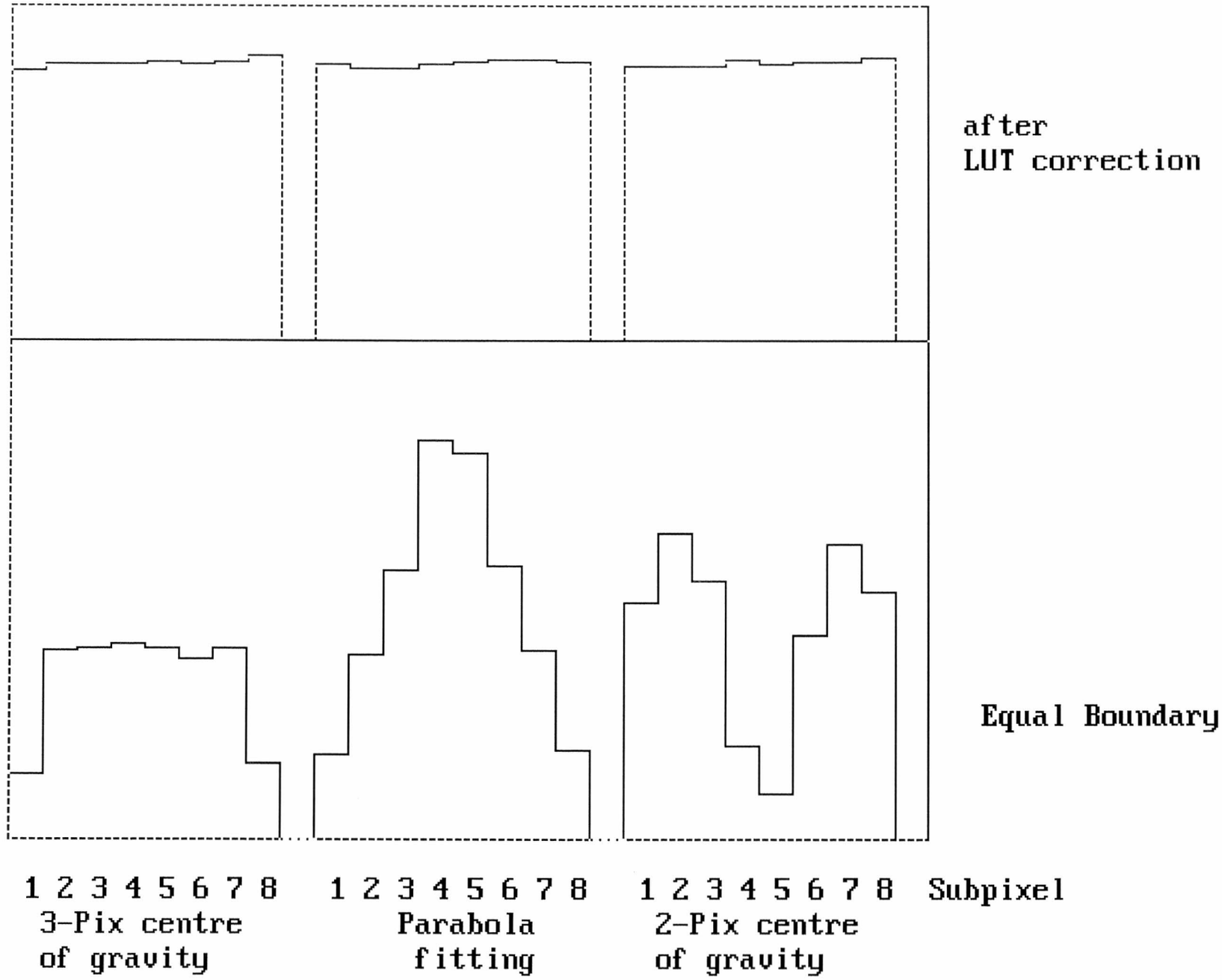

Fig. 15 Fixed patterns after LUT's correction

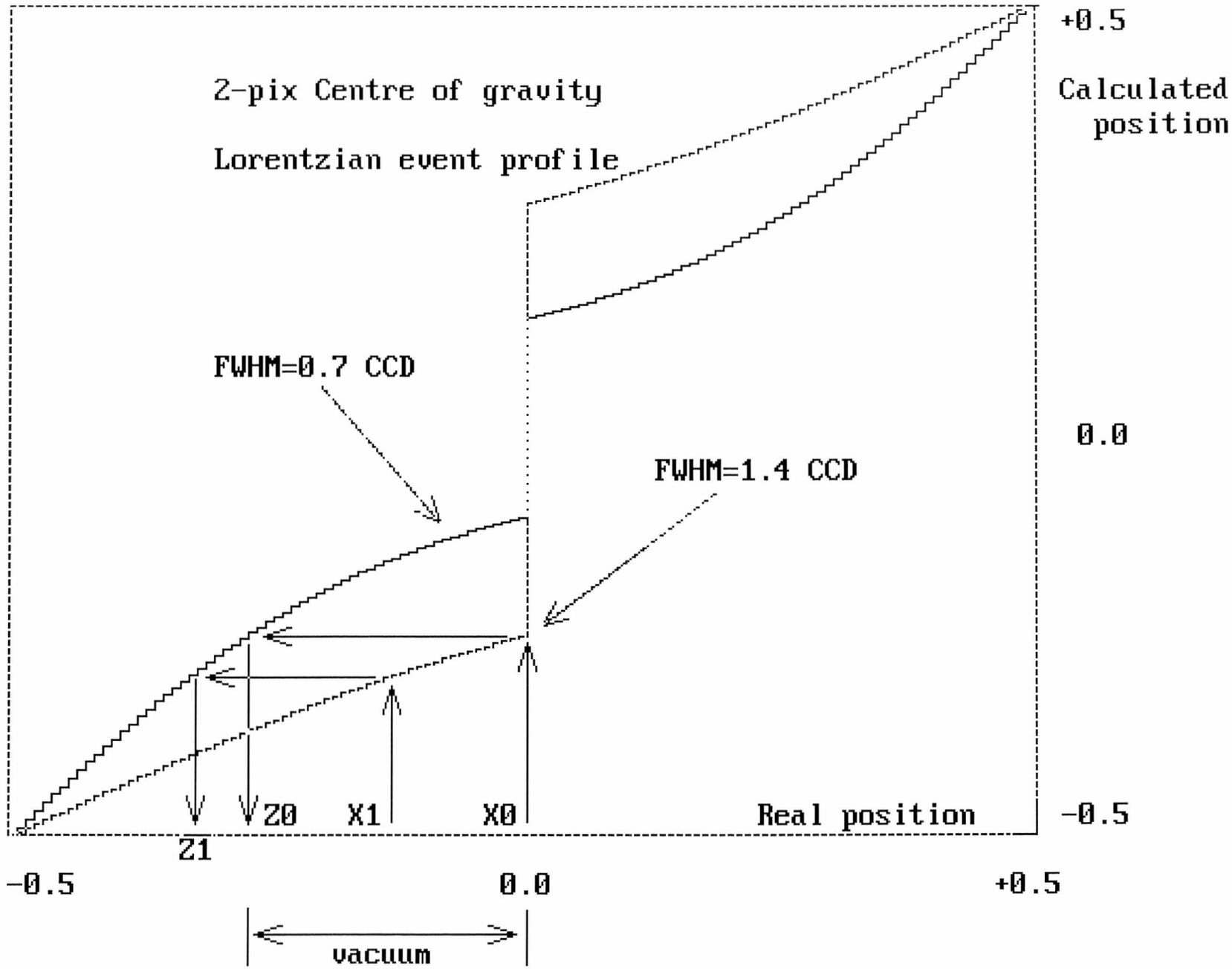

Fig. 16 Effect of discontinuity on centroiding image

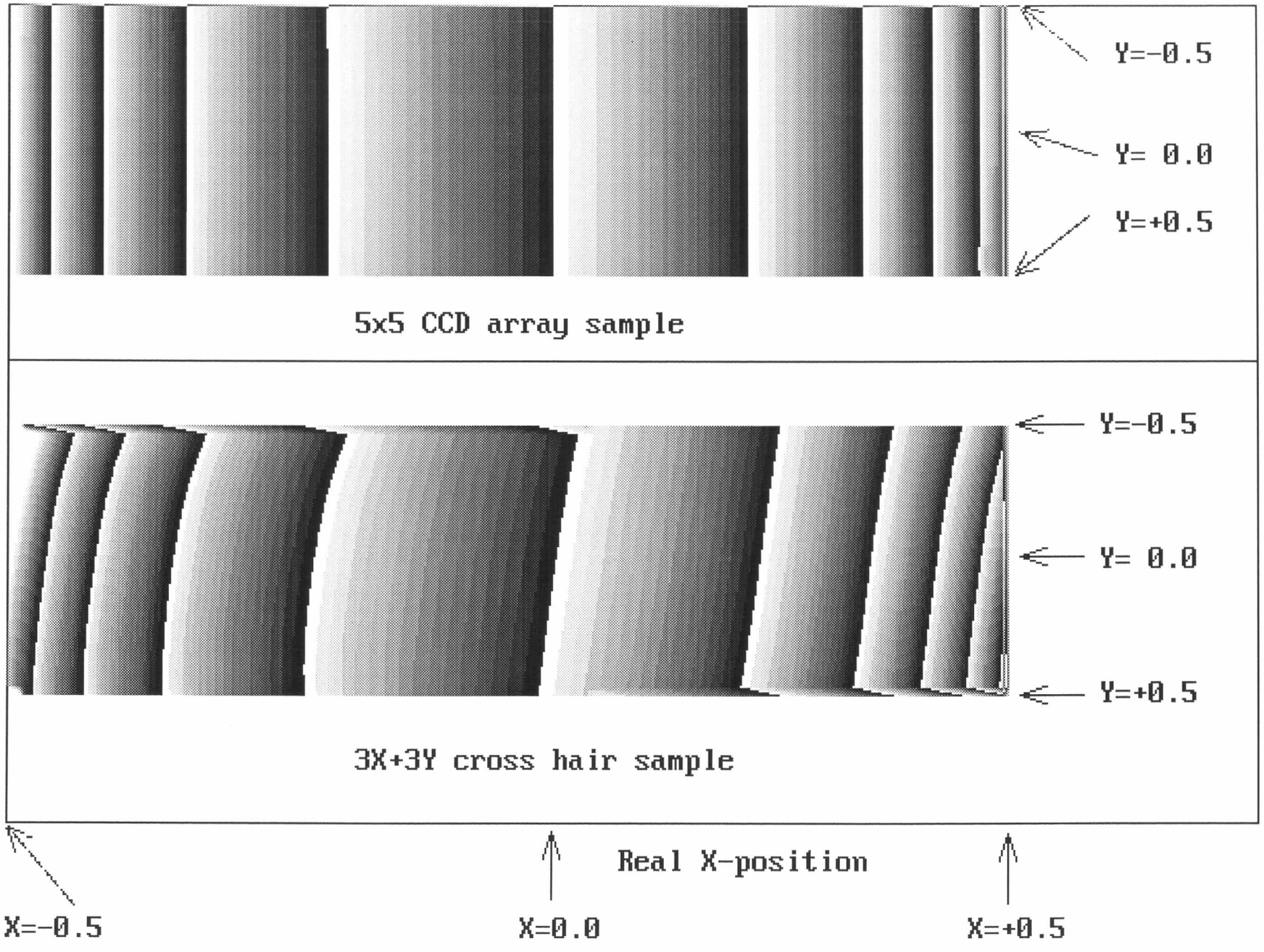

Fig. 17 Gray scale contour map of 2-dimension characteristic curve

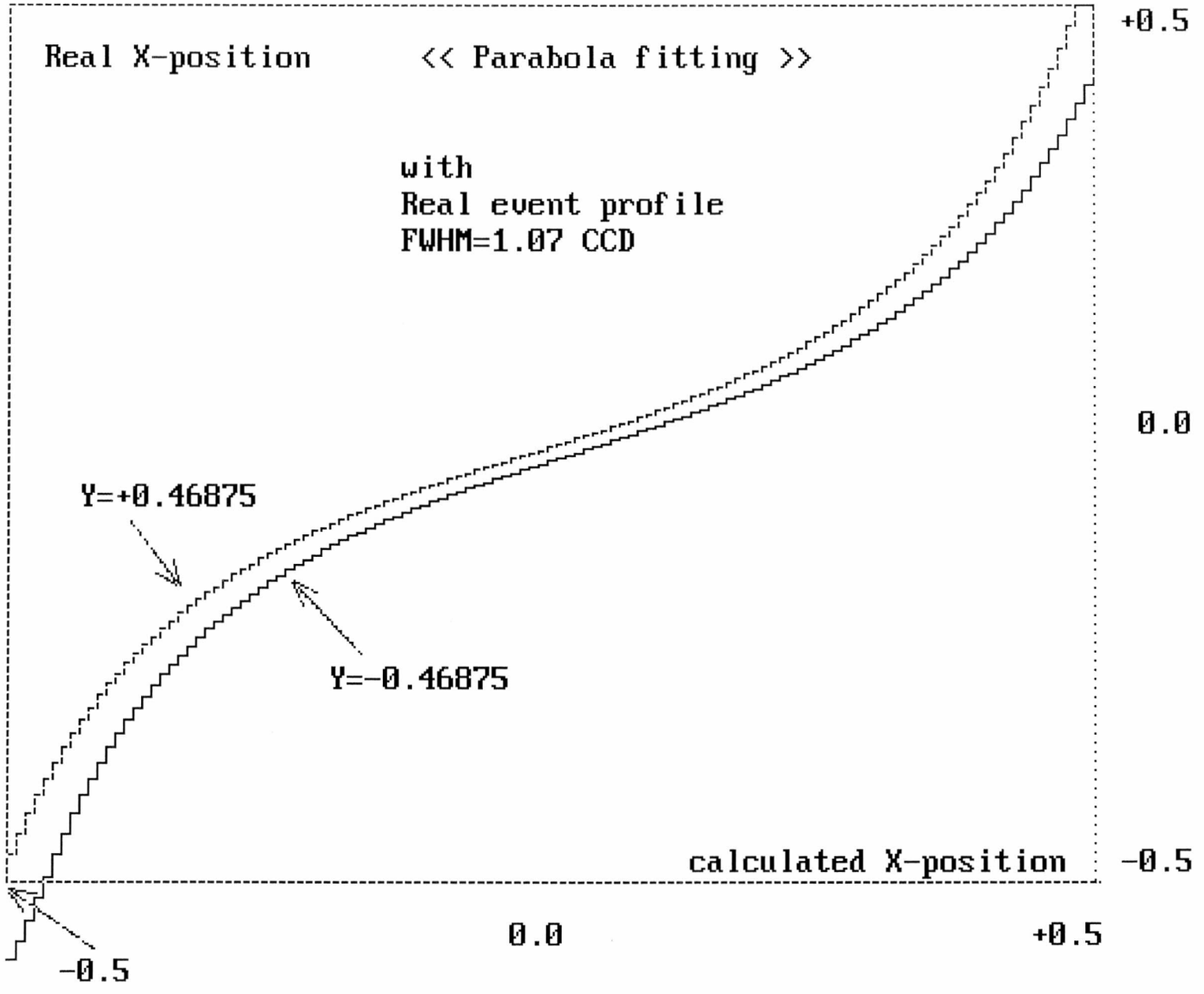

Fig. 18 Variation of characteristic curve along Y-direction

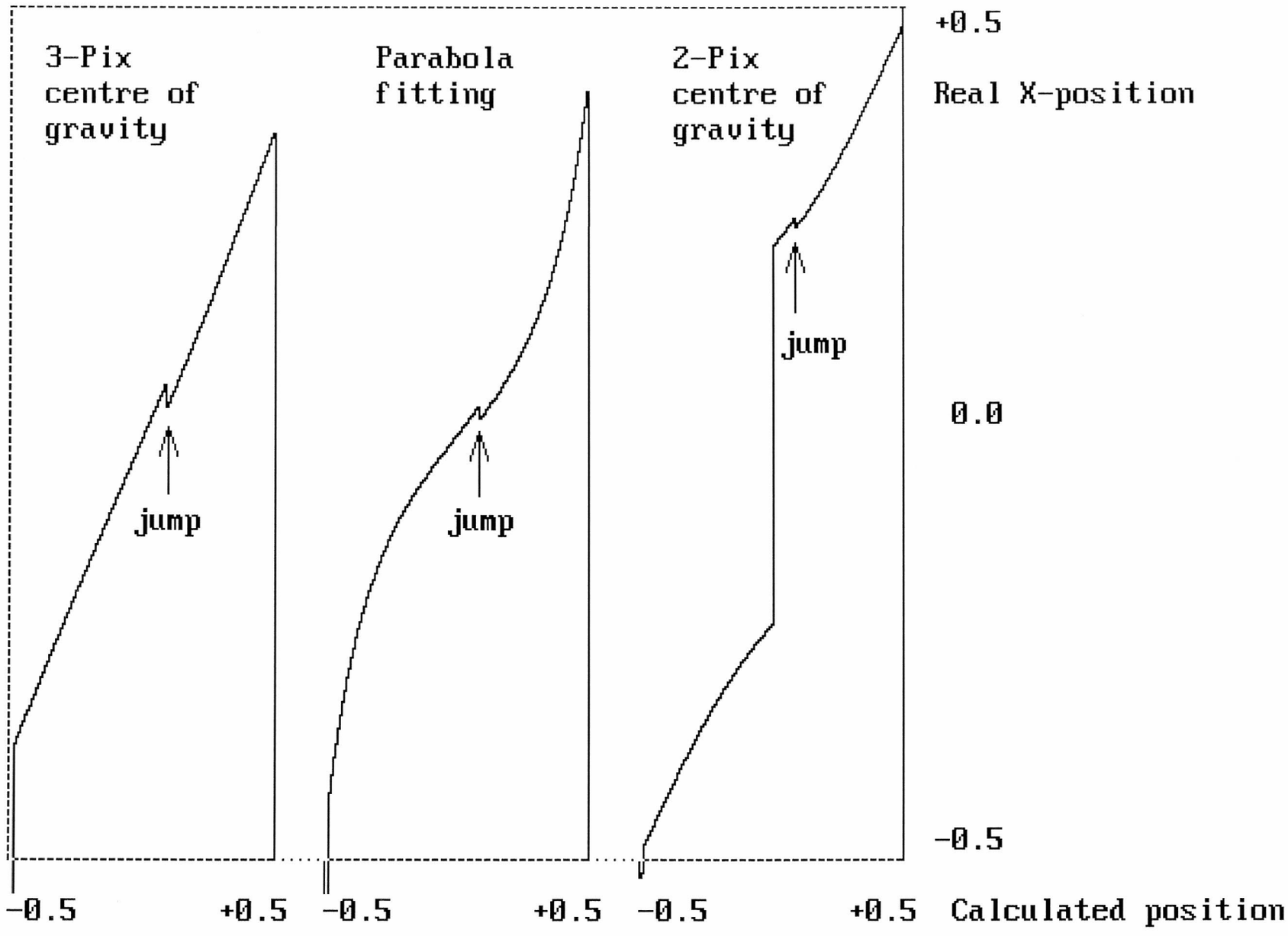

Fig. 19 Discontinuity in characteristic curves due to transition of smapling CCD pixels

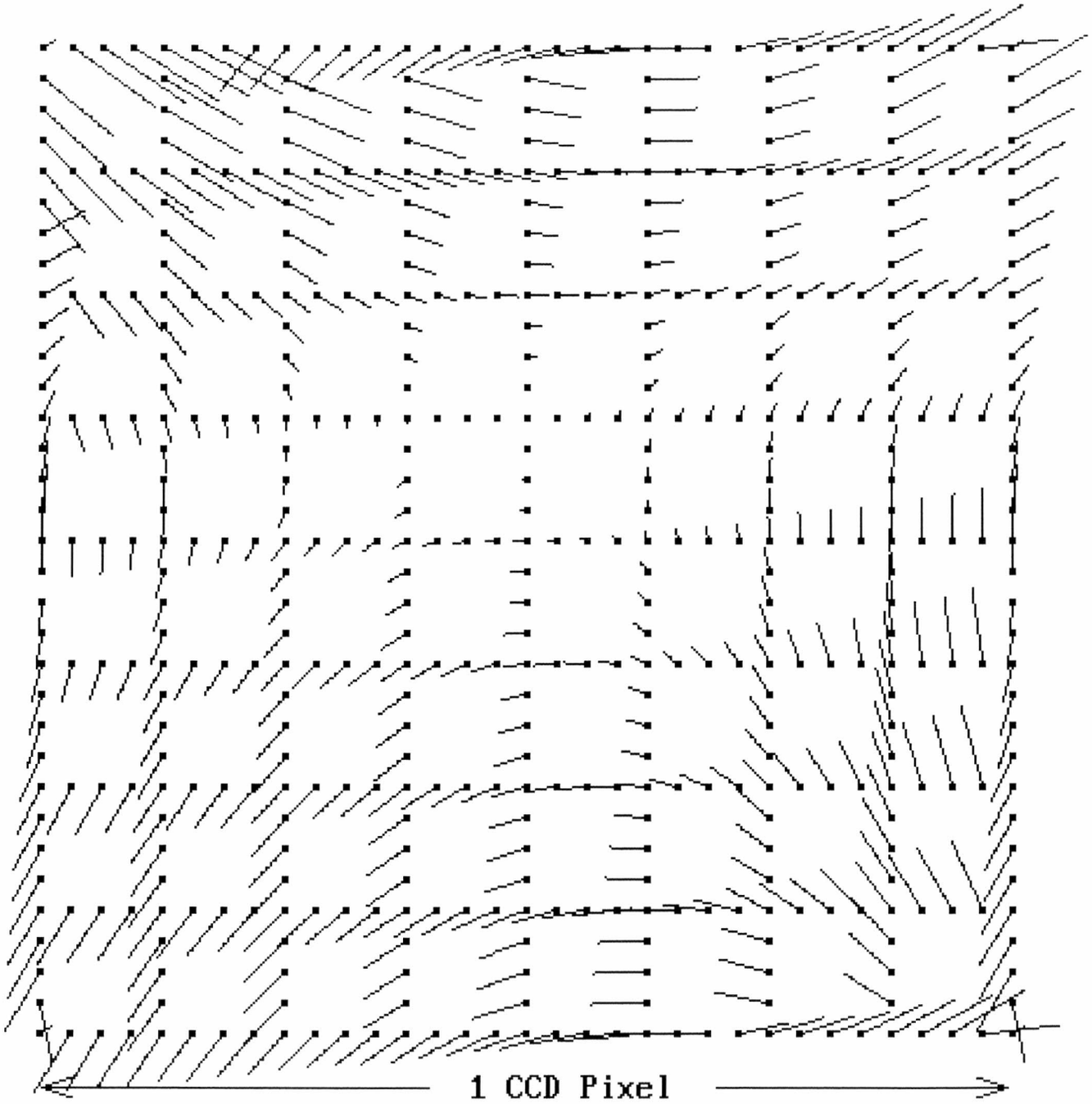

Fig. 20
Displacement of subpixel boundary

Parabola fitting

1-dim LUT

right event size
FWHM=1.07 CCD

displacement scale
x 3.0 times

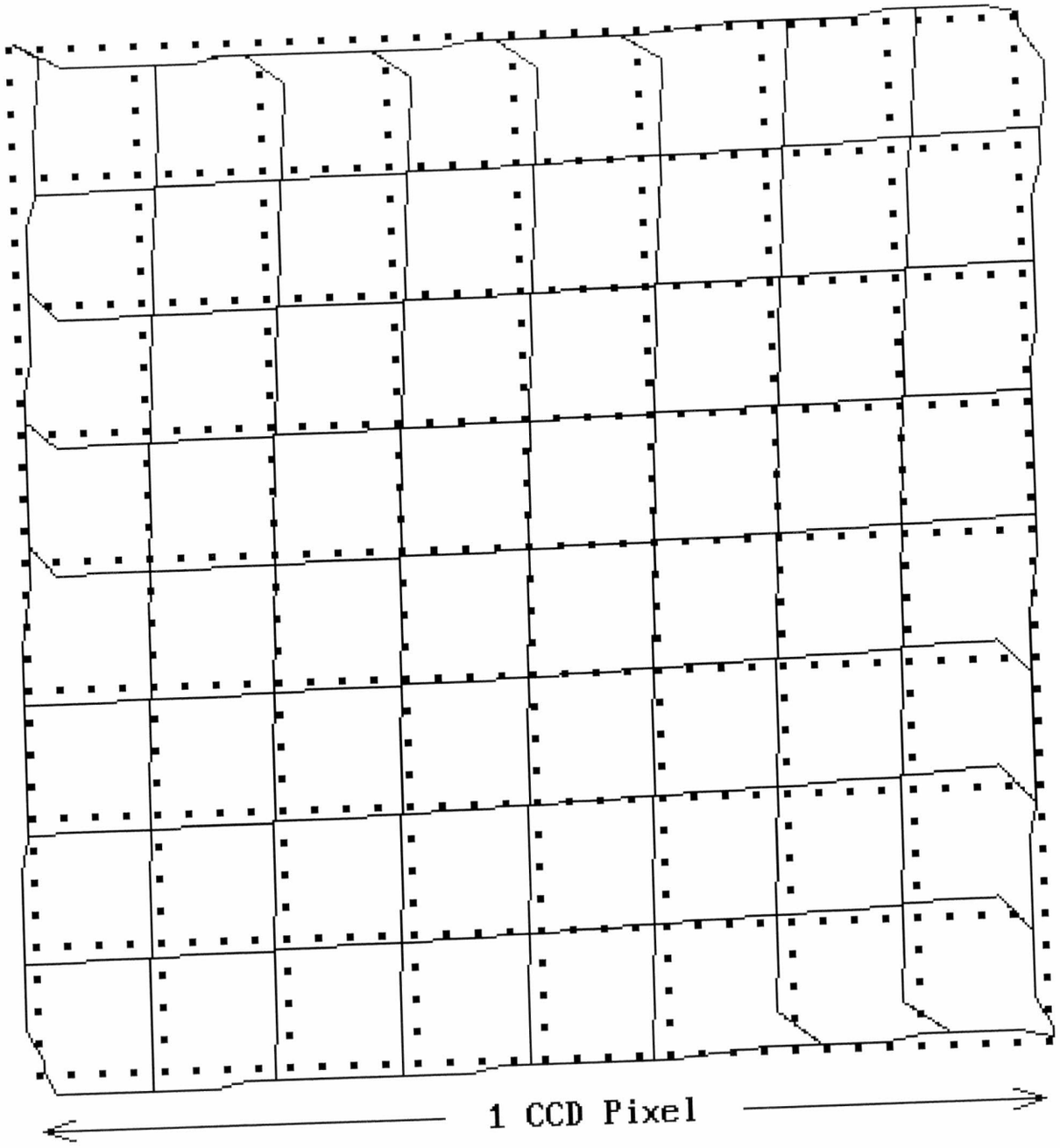

Fig. 21
True geometry of subpixel boundary

3-Pix centre of gravity

1-dim LUT

right event size FWHM=1.07 CCD

event profile from DEP_#8 tube

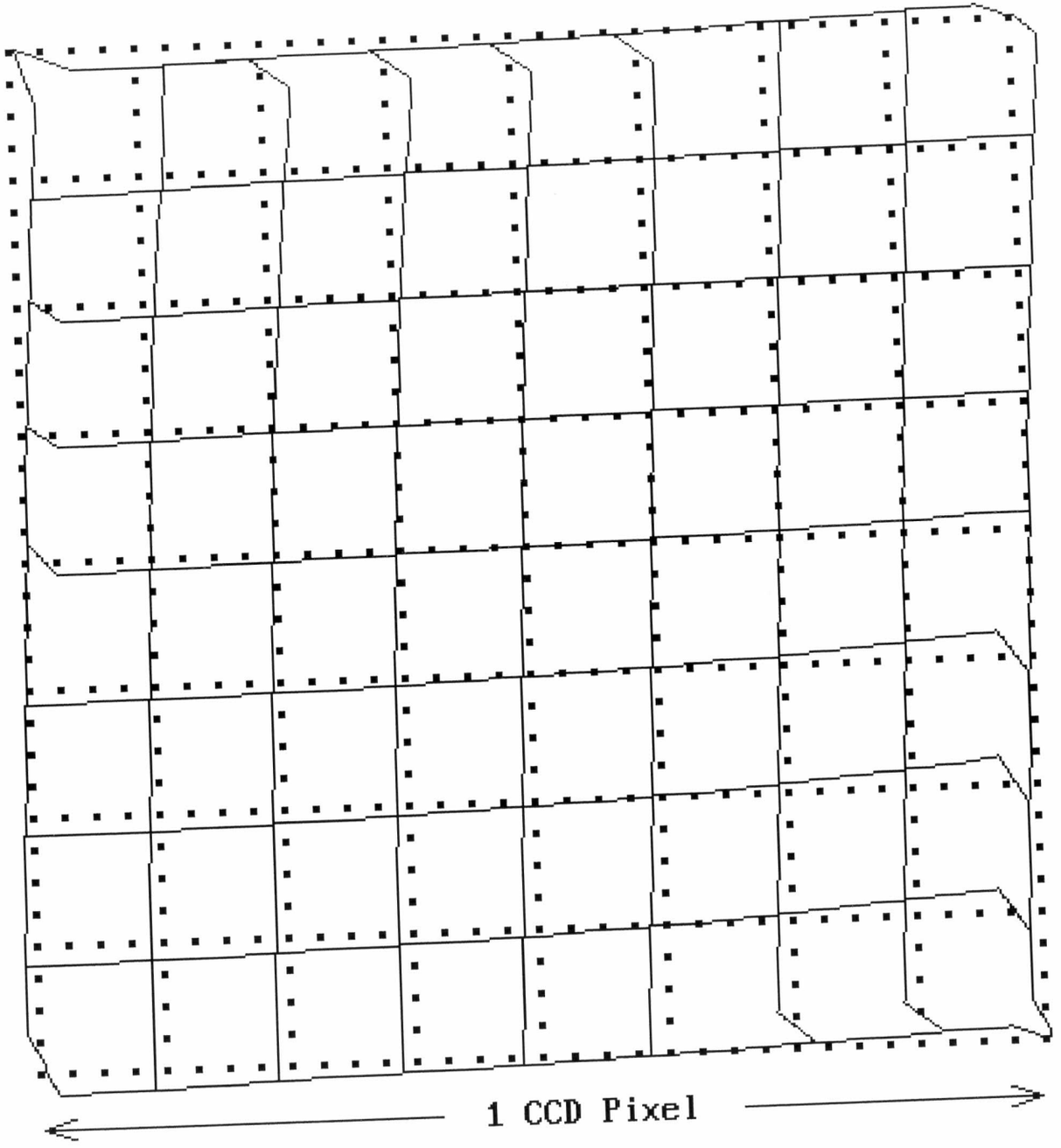

Fig. 22
True geometry of subpixel boundary

Parabola fitting

1-dim LUT

right event size
FWHM=1.07 CCD

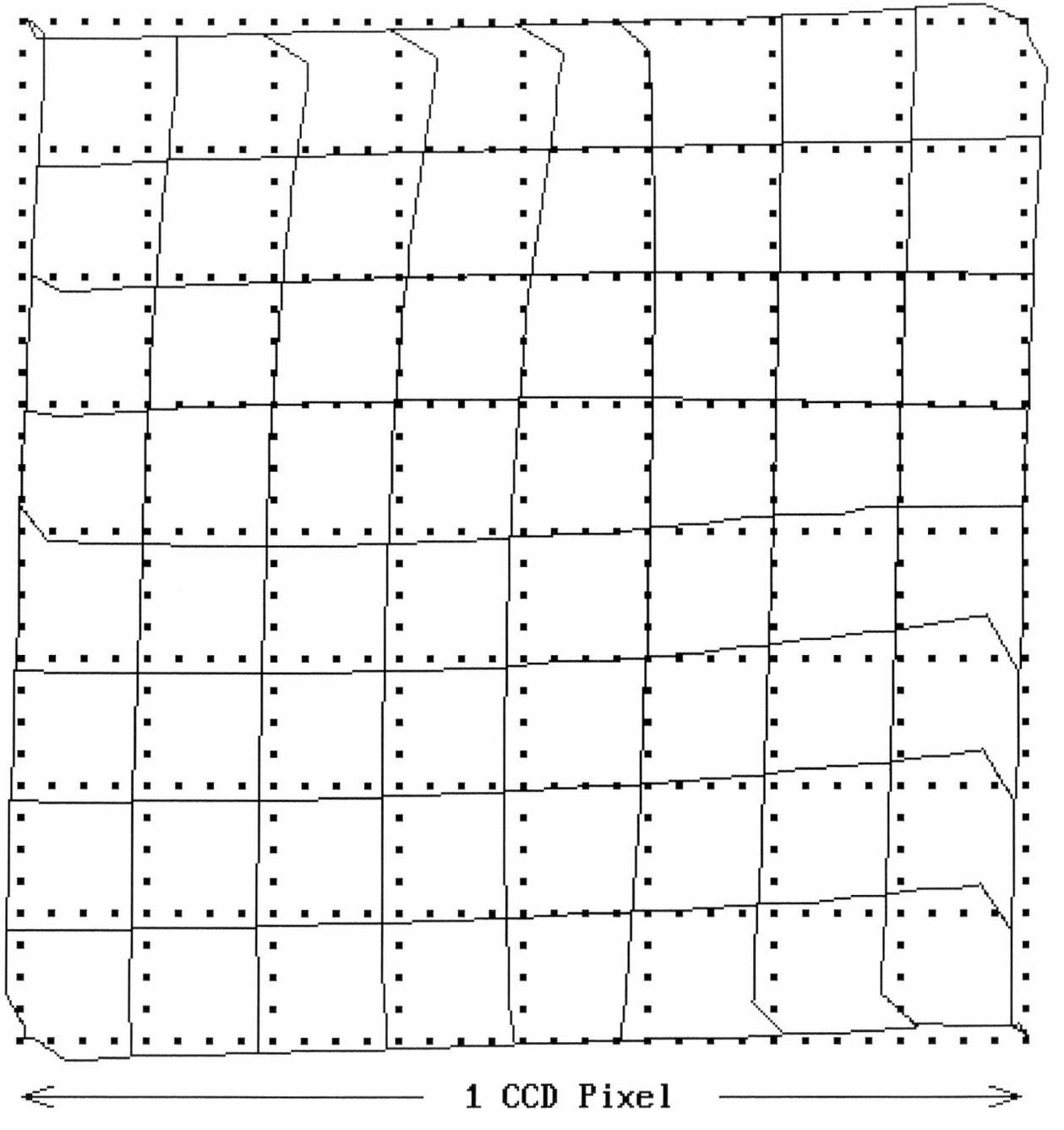

Fig. 23
True geometry of subpixel boundary

2-Pix centre of gravity

1-dim LUT

right event size
FWHM=1.07 CCD

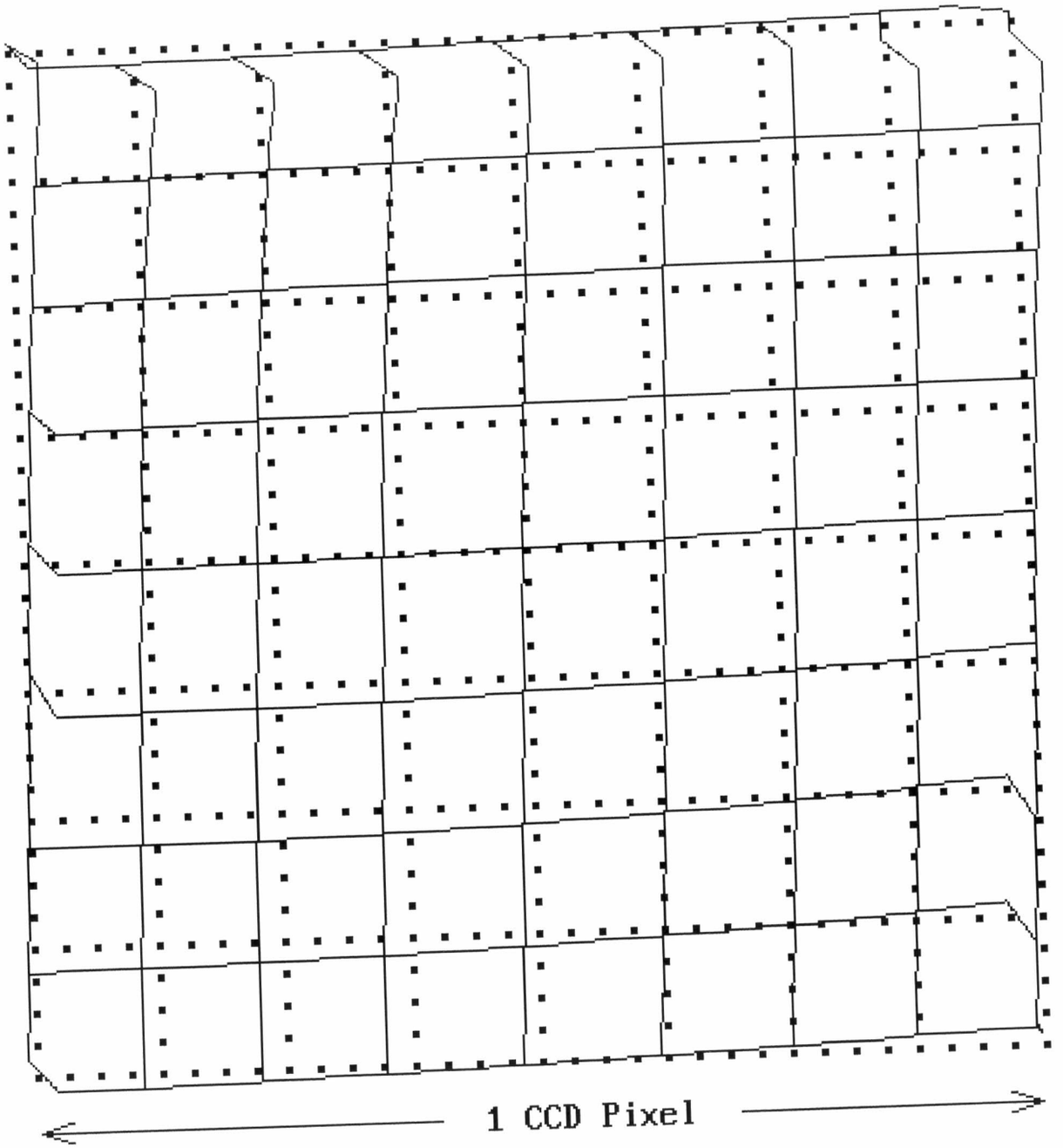

Fig. 24
True geometry of subpixel boundary

Parabola fitting

1-dim LUT x2

for small event
FWHM=0.95 CCD

LUTs were tuned
to FWHM=1.07 CCD

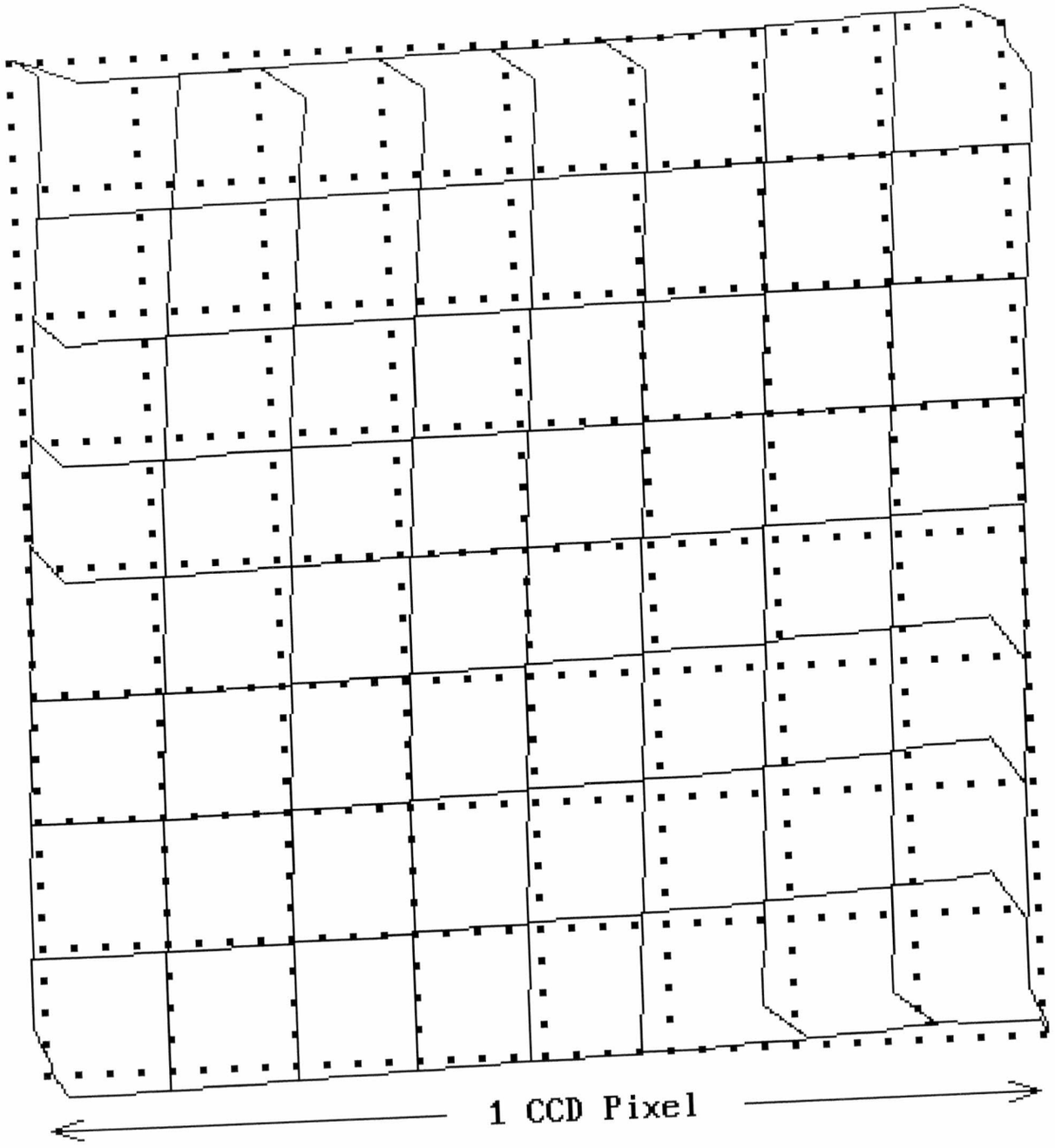

Fig. 25
True geometry of subpixel boundary

Parabola fitting

1-dim LUT x2

for large event
FWHM=1.20 CCD

LUTs were tunned
to FWHM=1.07 CCD

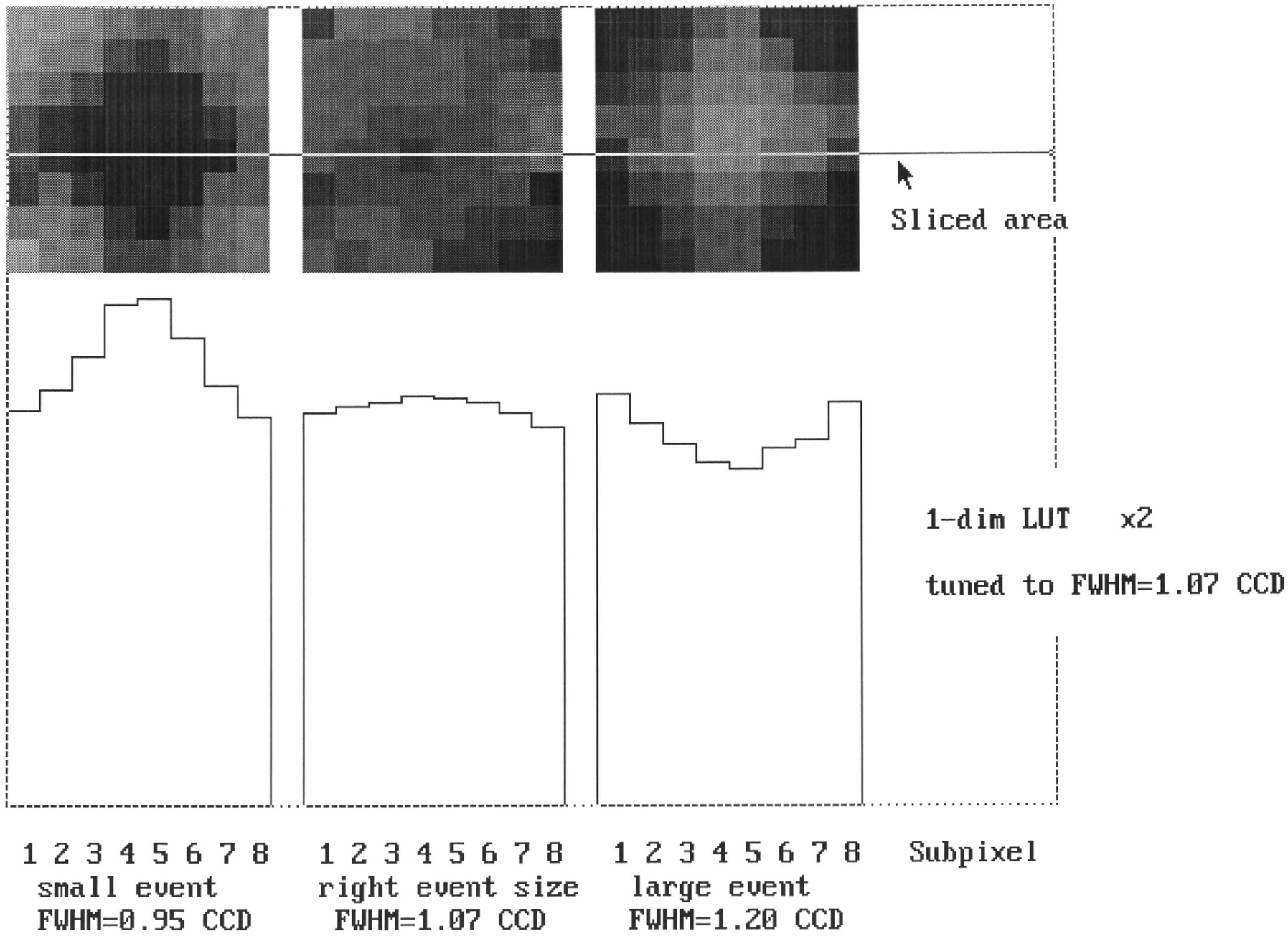

Fig. 26 2-dimension fixed pattern for various event size

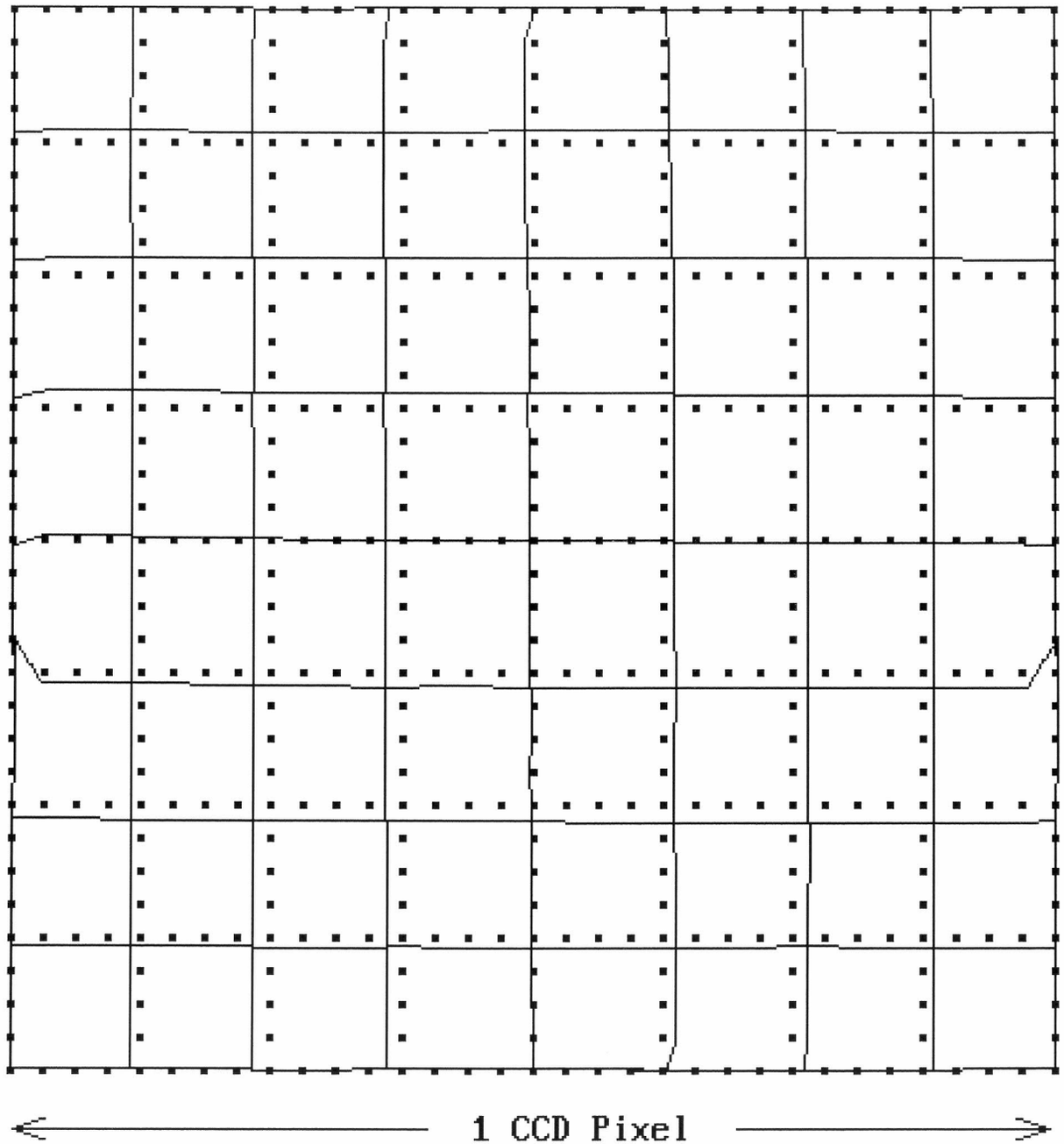

Fig. 27
True geometry of
subpixel boundary

Parabola fitting

~~1~~ 2-dim LUT

for small event
FWHM=0.95 CCD

LUT was tunned to
FWHM=1.07 CCD

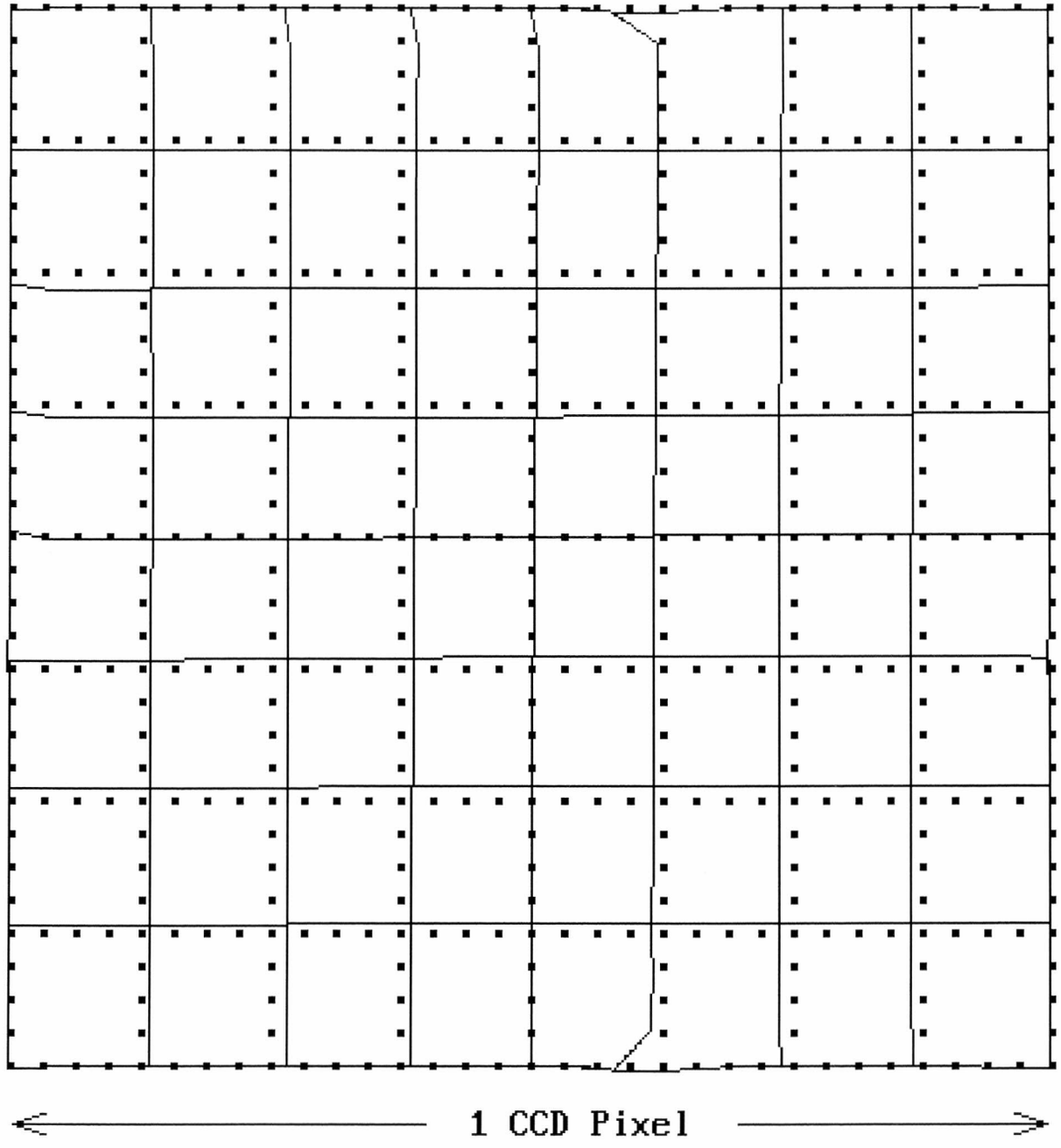

Fig. 28
True geometry of subpixel boundary

Parabola fitting

2-dim LUT

for large event
FWHM=1.20 CCD

LUT was tuned to
FWHM=1.07 CCD

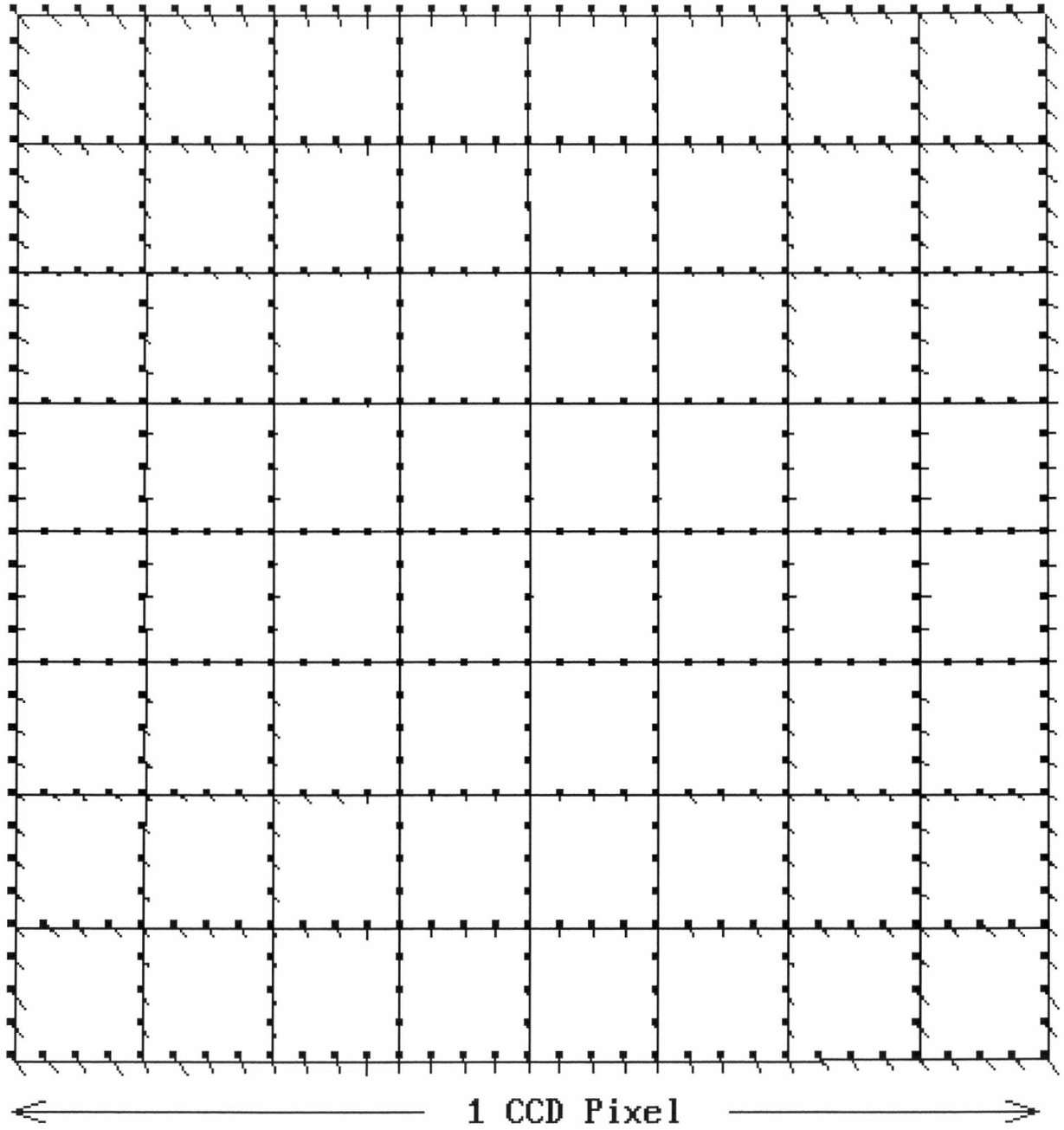

Fig. 29
True geometry of
subpixel boundary

Parabola fitting

5x5 sample
1-dim LUT

right event size
FWHM=1.07 CCD

Displacement scale
x 3.0 times

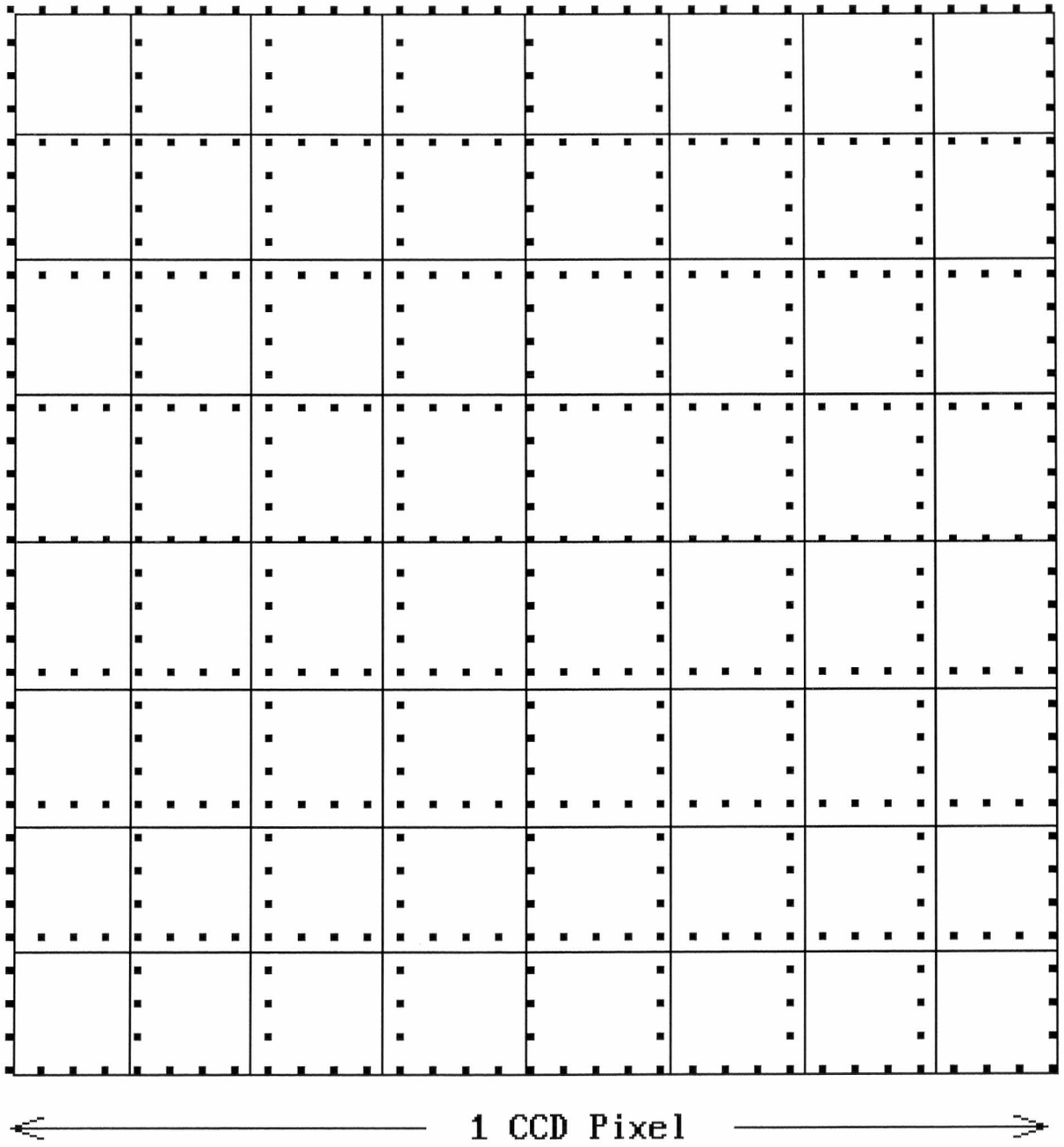

Fig. 30
True geometry of
subpixel boundary

Parabola fitting

5x5 CCD sample
1-dim LUT x2

for small event
FWHM=0.95 CCD

LUTs were tuned
to FWHM=1.07 CCD

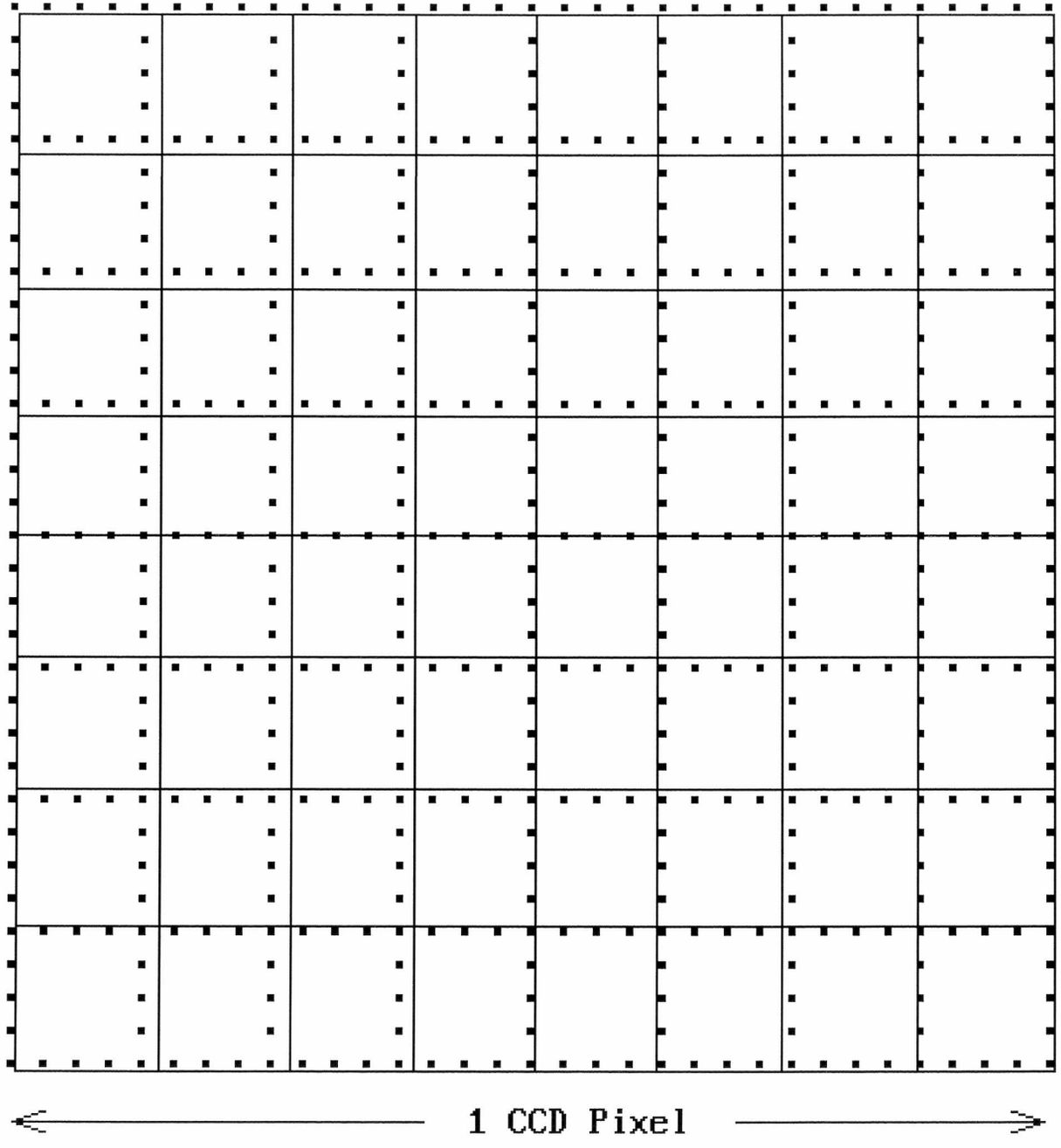

Fig. 31
True geometry of
subpixel boundary

Parabola fitting

5x5 CCD sample
1-dim LUT x2

for large event
FWHM=1.20 CCD

LUTs were tuned
to FWHM=1.07 CCD

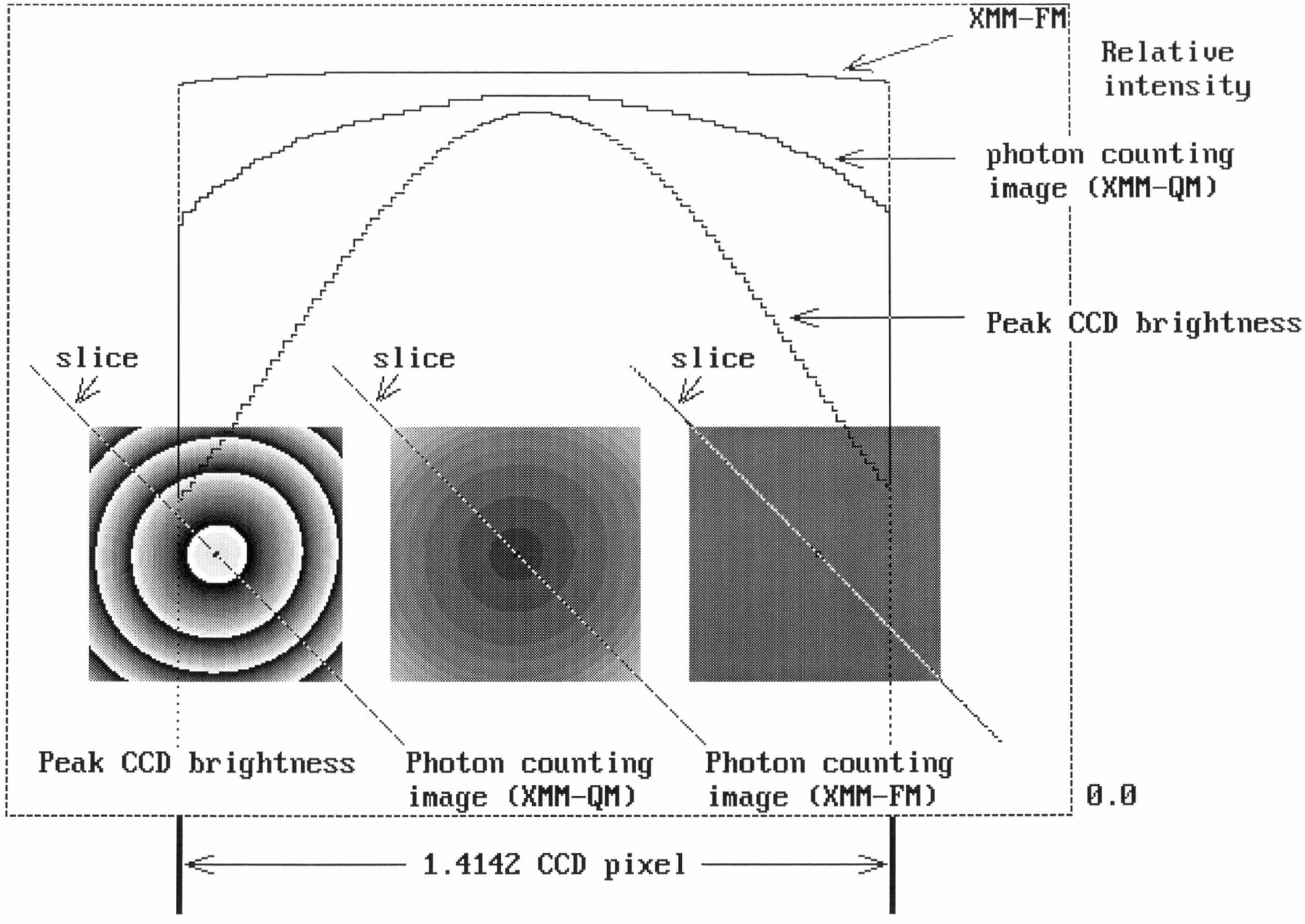

Fig. 32 Brightness variation along a CCD pixel

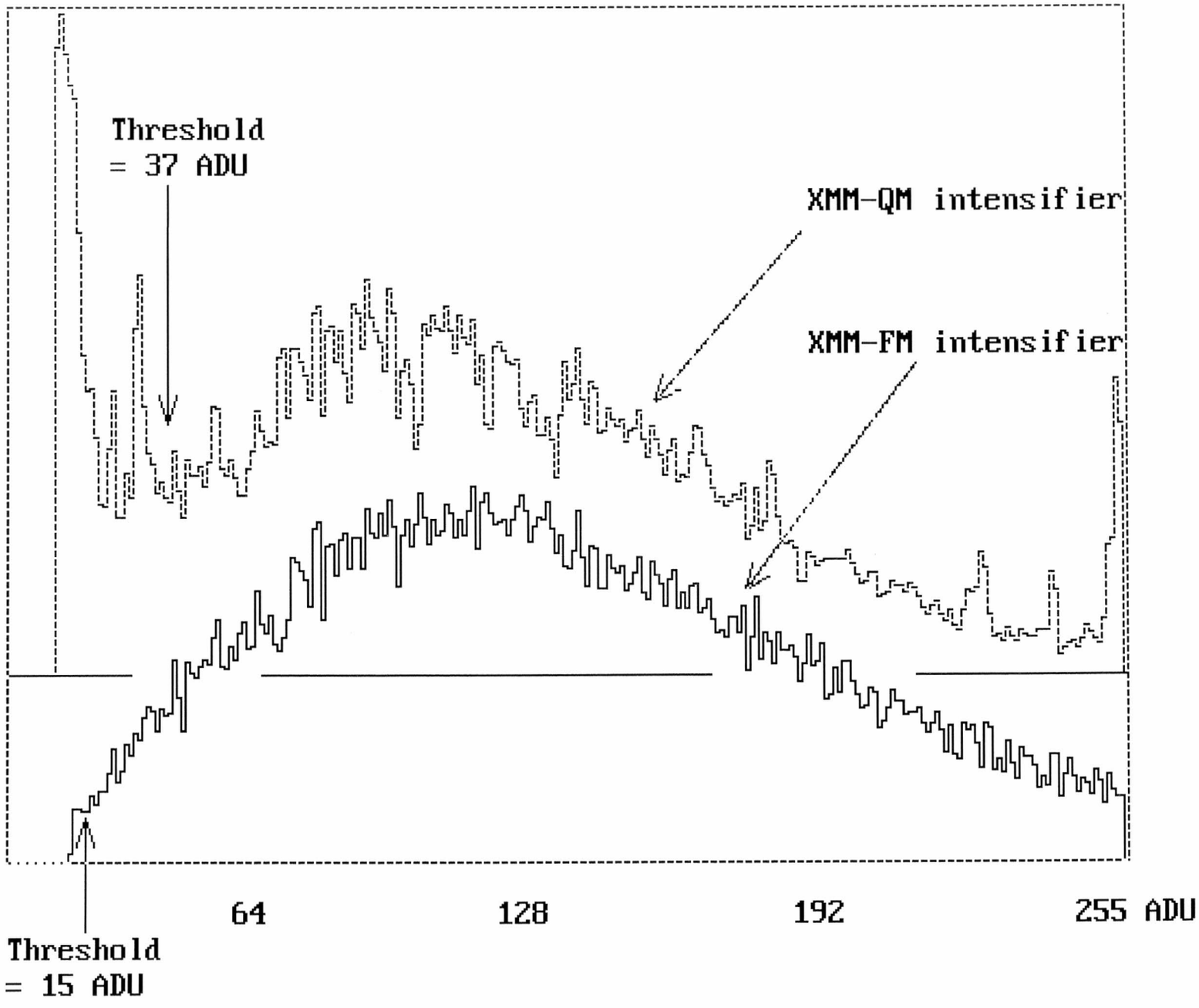

Fig. 33 Low noise and deep valley of XMM-FM tube in pulse height distribution

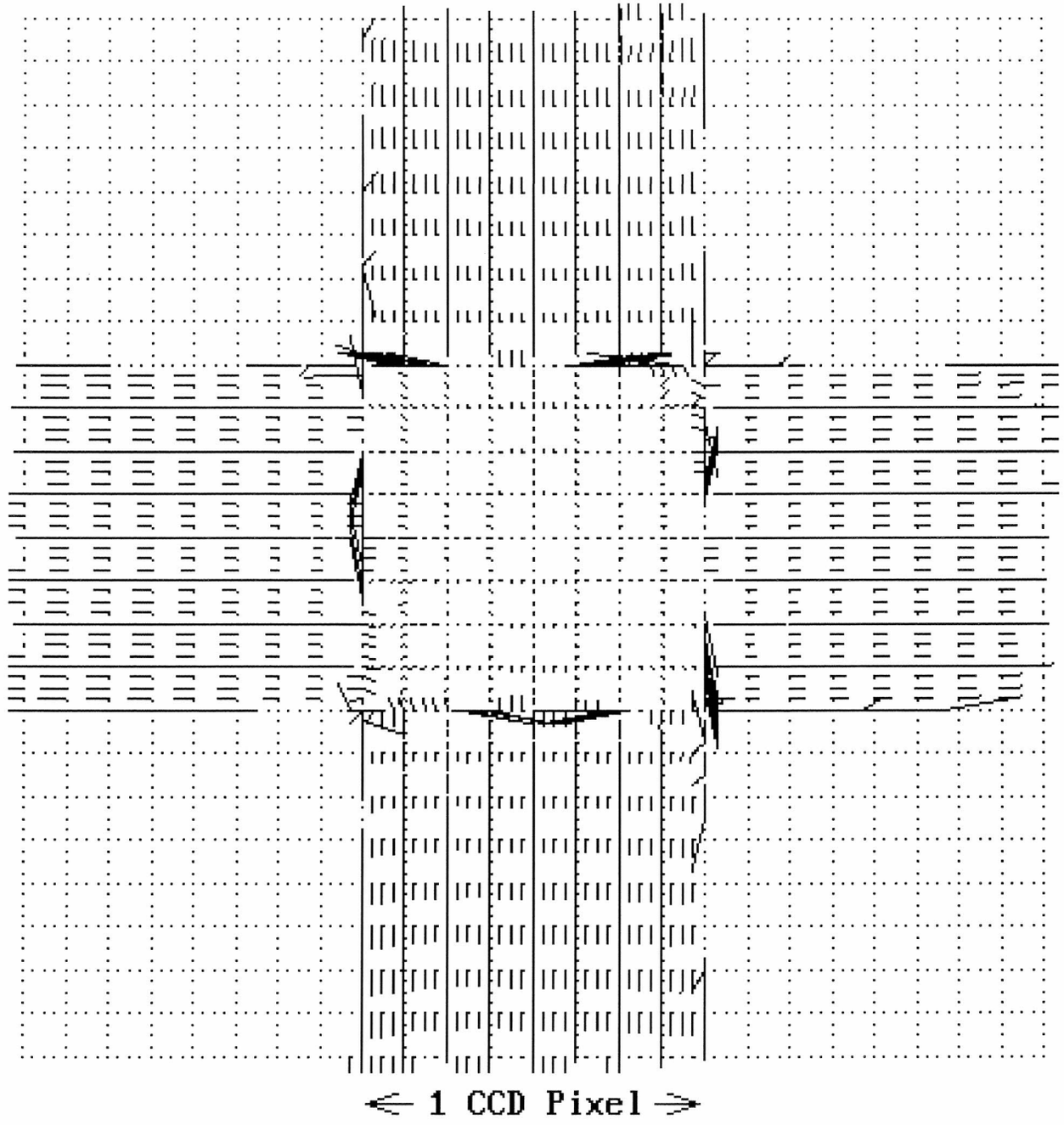

Fig. 34
Effect of hot pixel

3-Pix centre of gravity

Hot Pixel = 1 ADU

Scale of displacement vector is x5.0 times

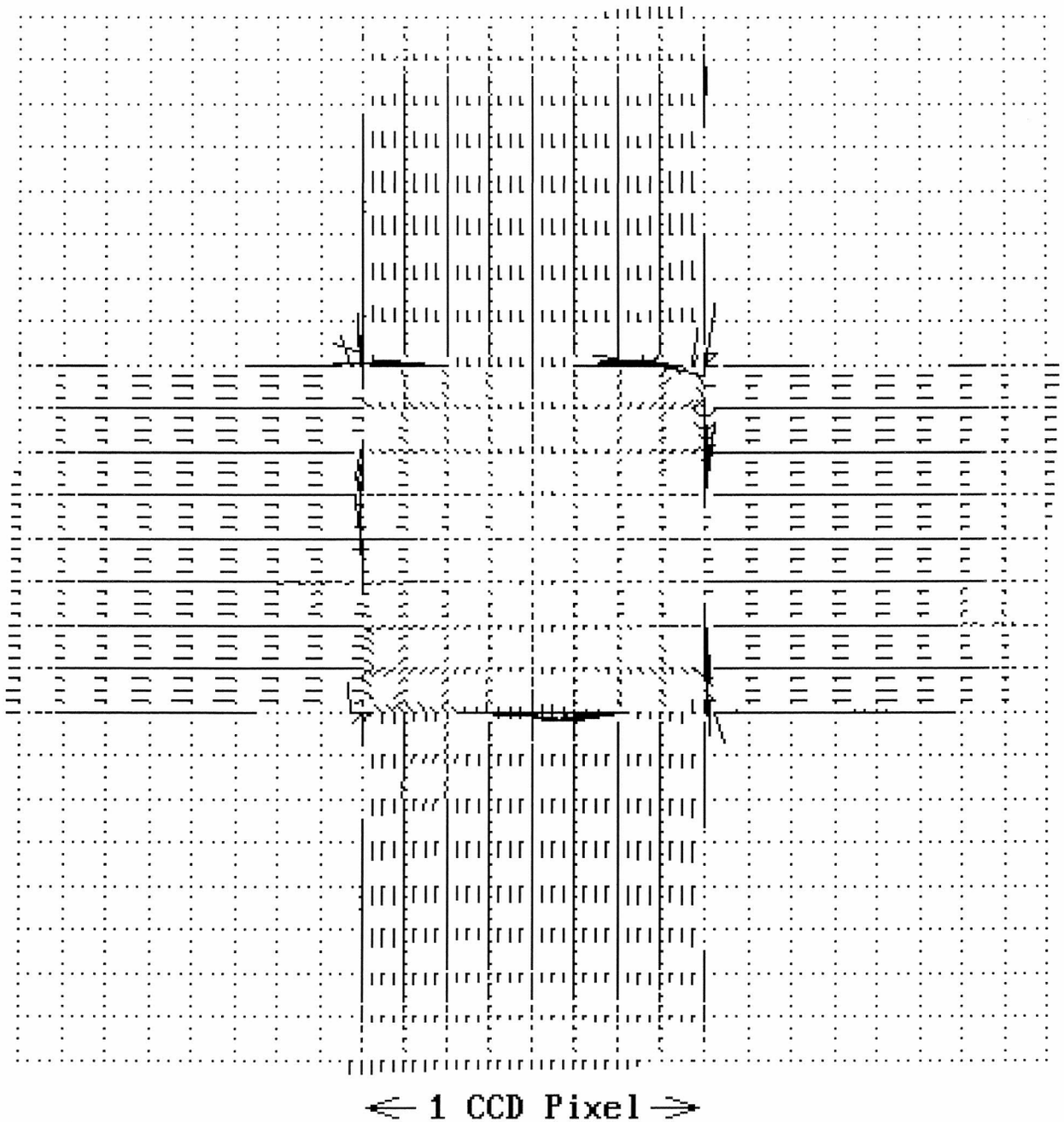

Fig. 35
Effect of hot pixel

Parabola fitting

Hot pixel = 1 ADU

Scale of
displacement vector
is x5.0 times

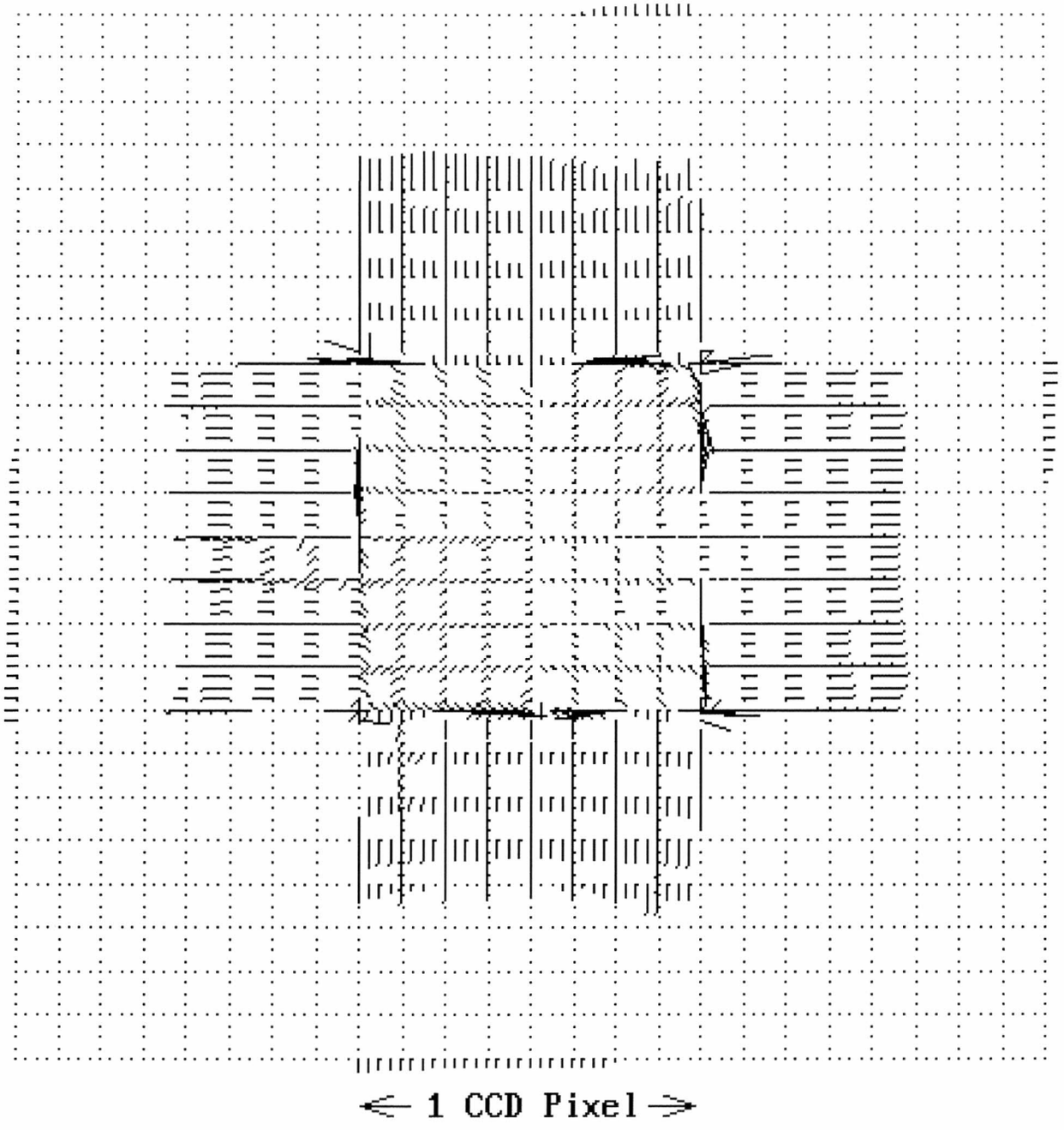

Fig. 36
Effect of hot pixel

2-Pix centre of gravity

Hot pixel = 1 ADU

Scale of displacement vector is x5.0 times

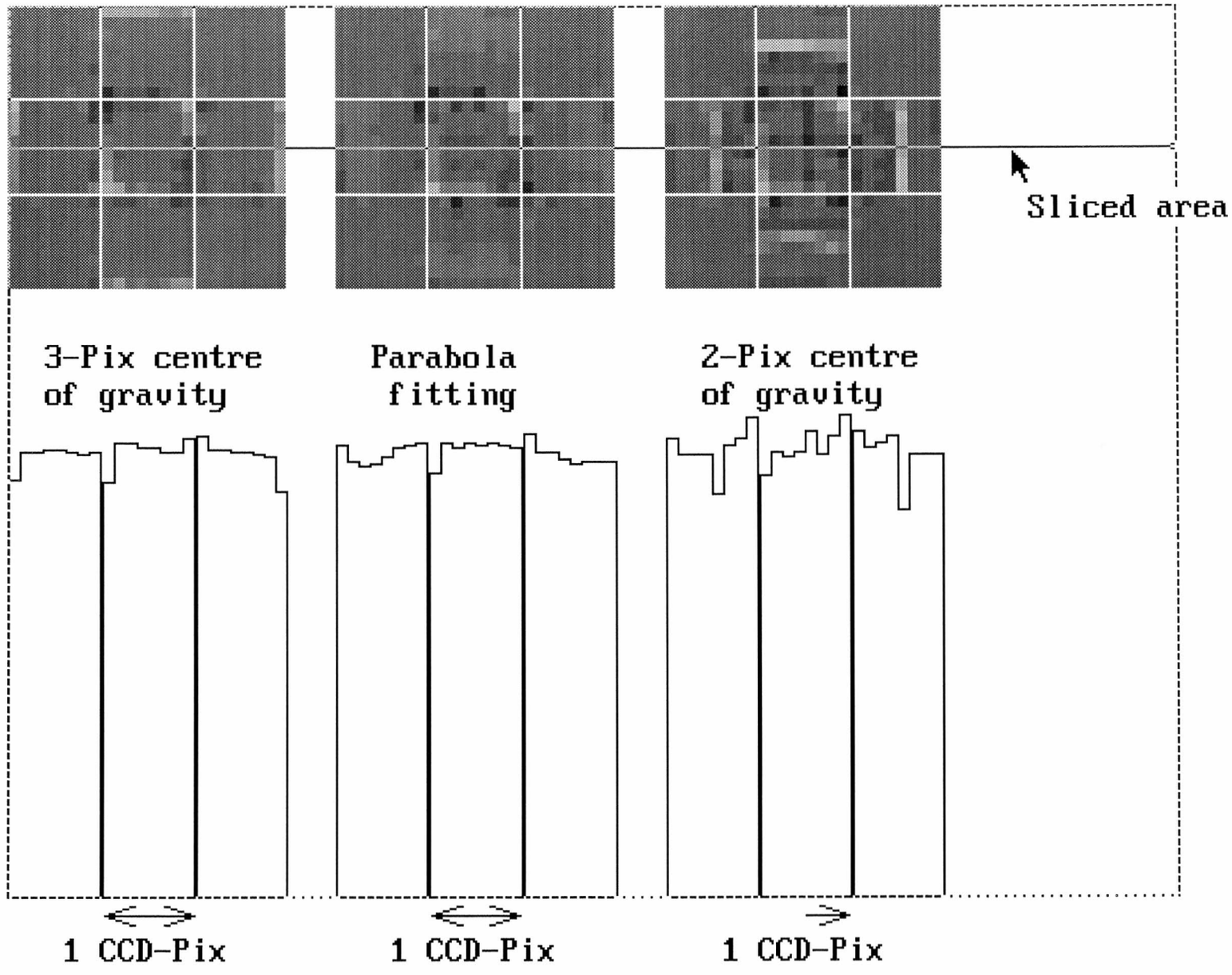

Fig. 37 Fixed pattern caused by a hot pixel (=1 ADU)

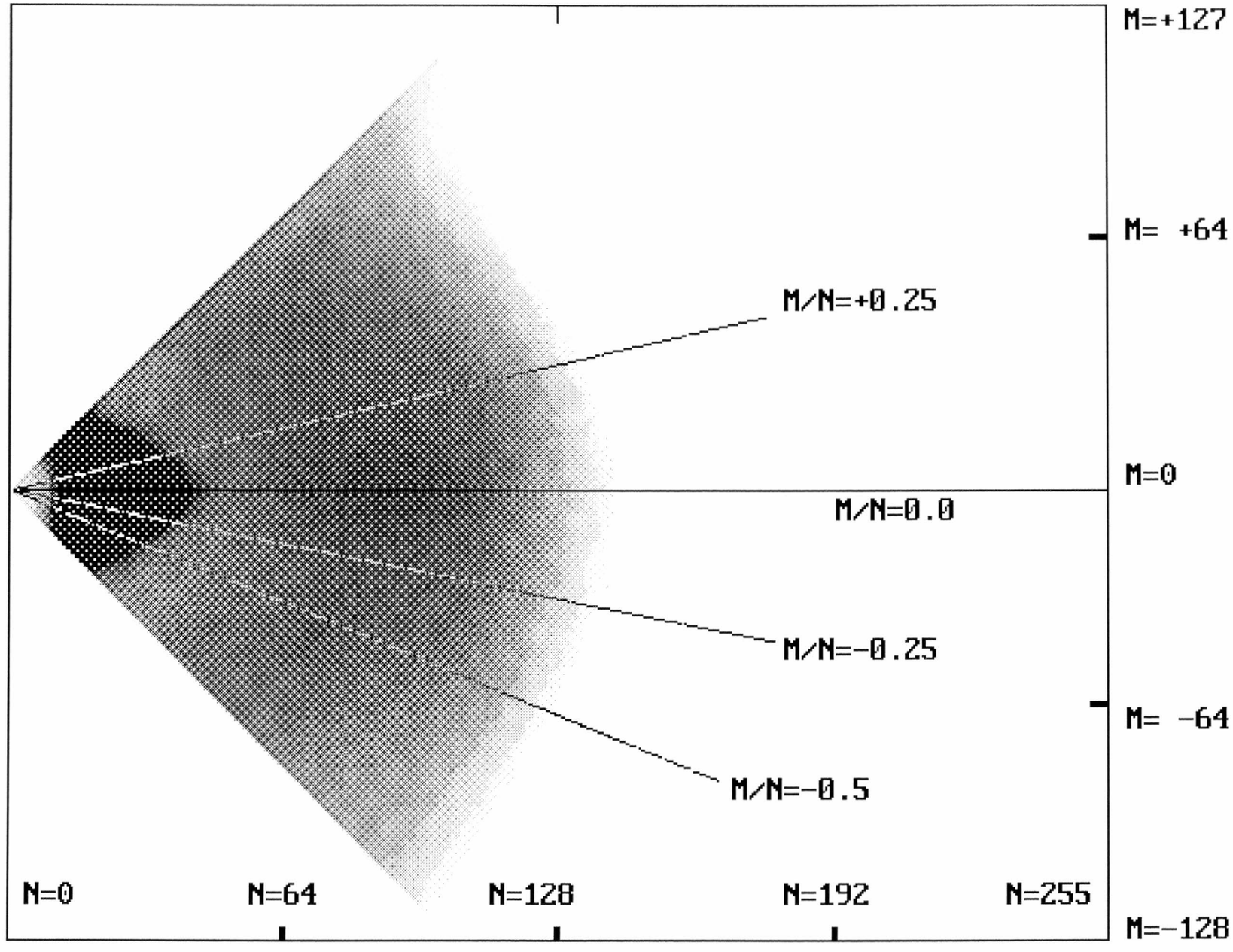

16H 17M 37S 16H 22M 37S 1997/09/05/

Fig. 38 M:N map for X-axis F-F 20,000 c/s with XMM-QM's BPE

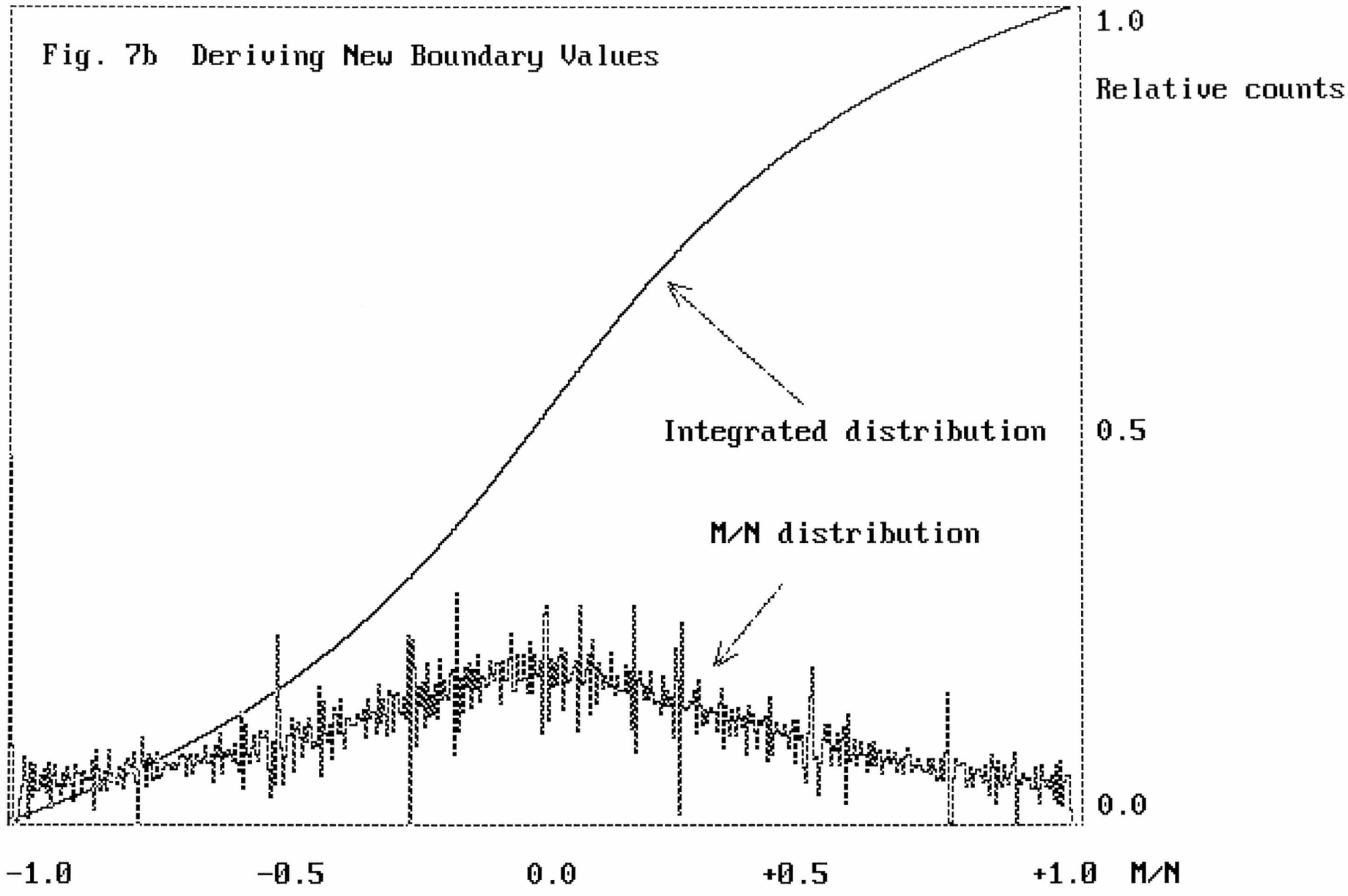

13H 34M 09S 13H 44M 09S 1997/09/07/

Fig. 39 M/N distribution with XMM-OM's QM BPE

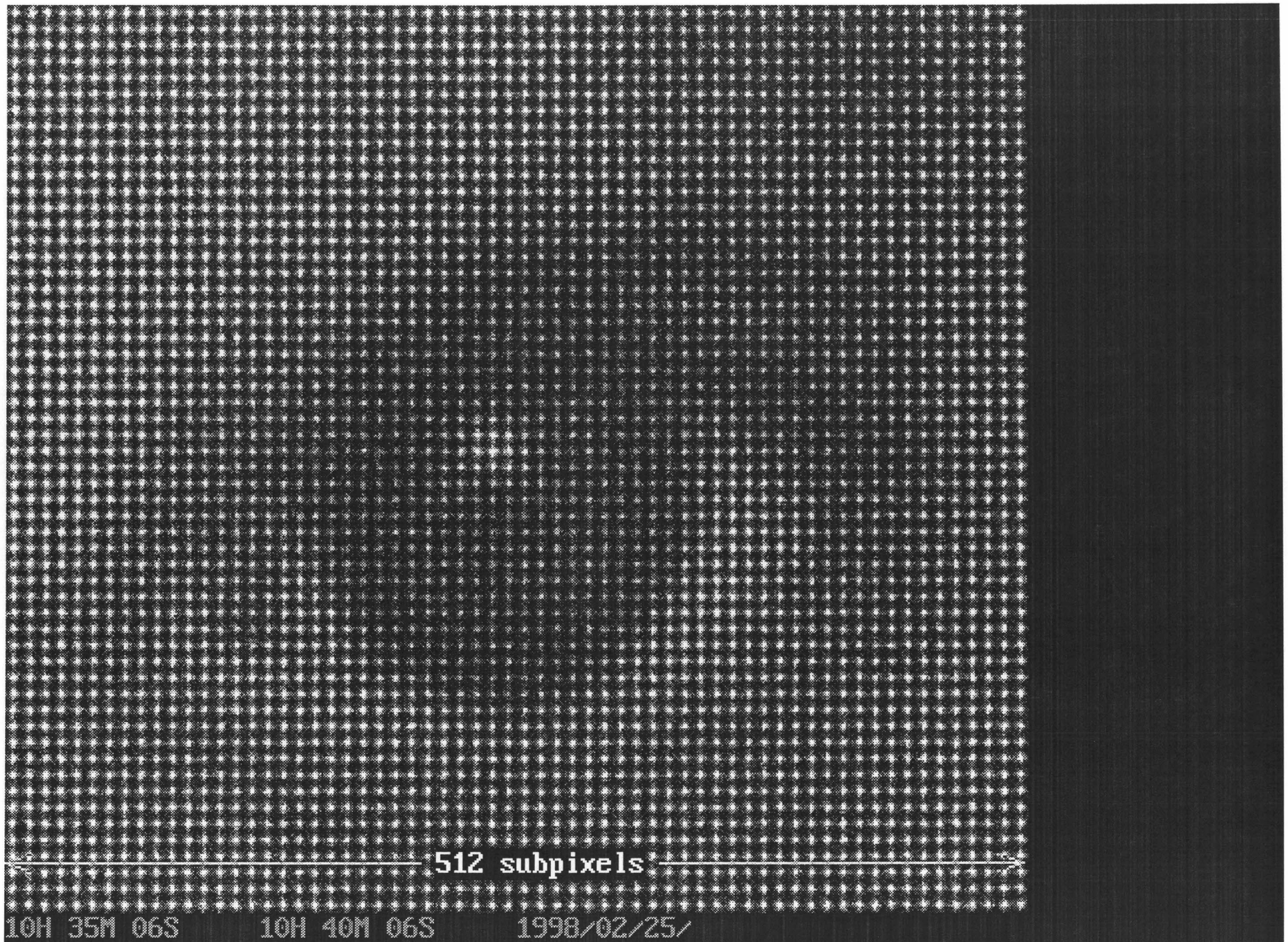

Fig. 40 Photon cointing image with Equal-boundaries Exp=300sec

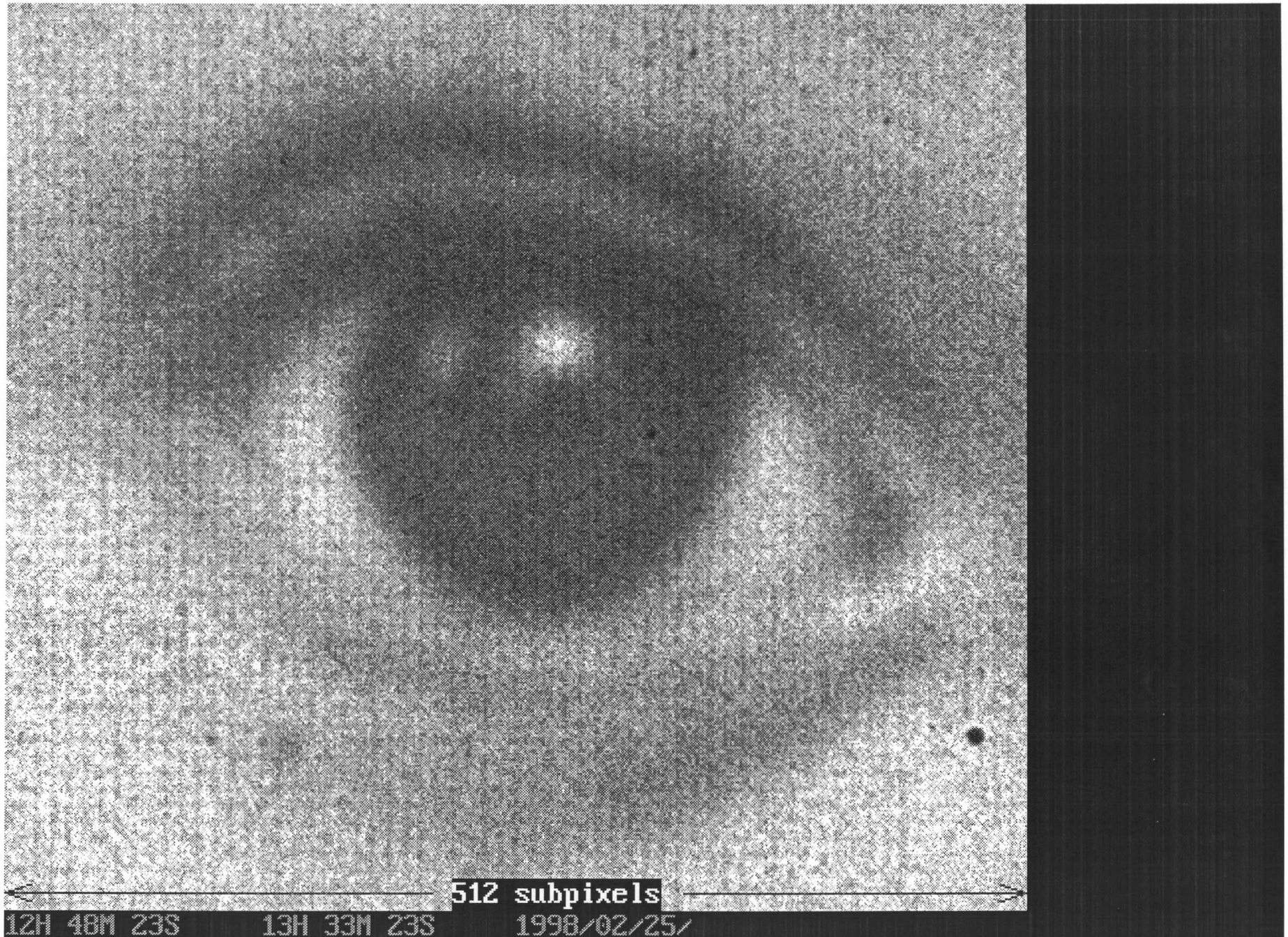

Fig. 41 Photon counting image with new boundaries from M/N distribution

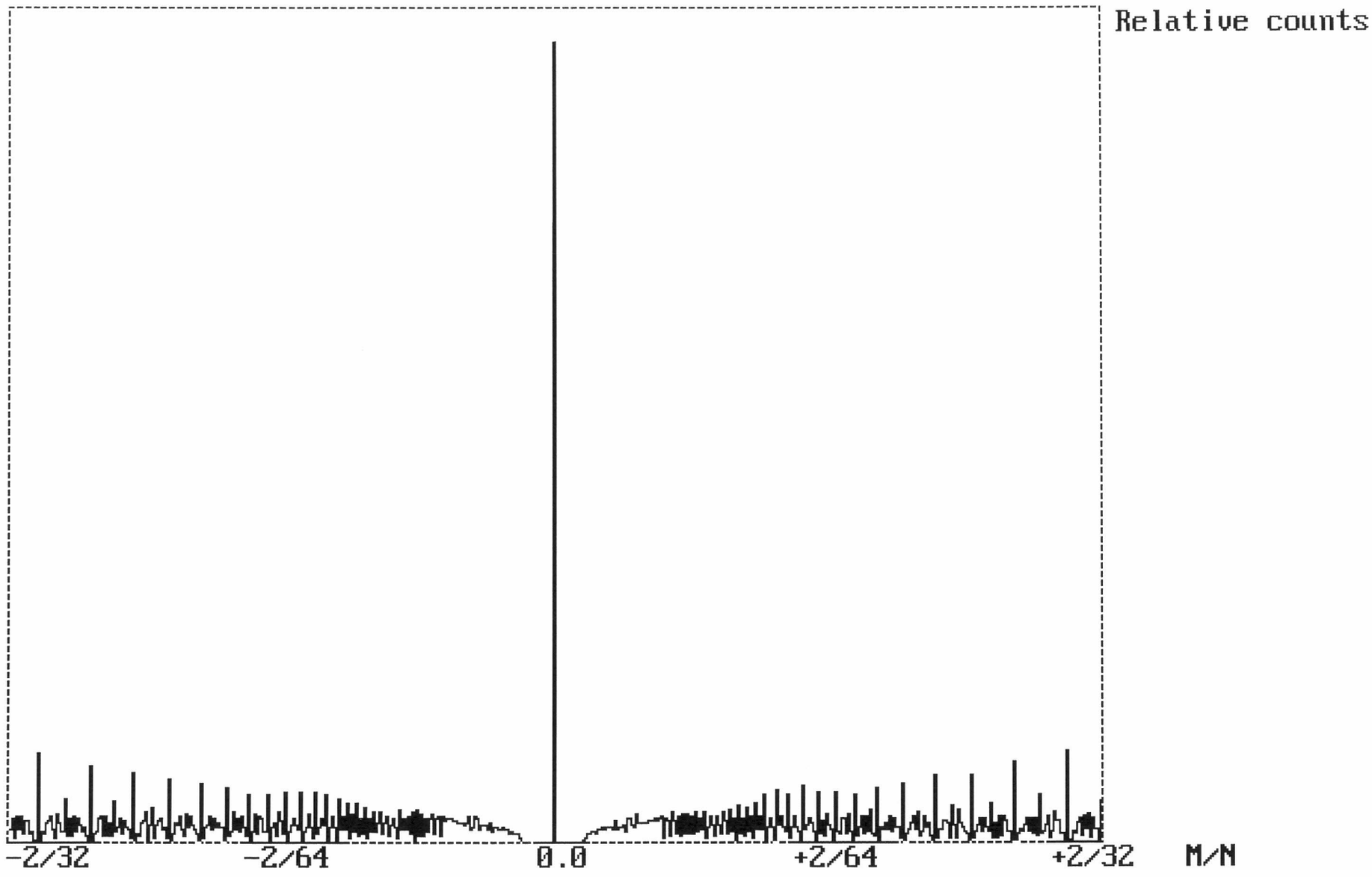

Fig. 42 M/N distribution near M/N=0 without randomizing

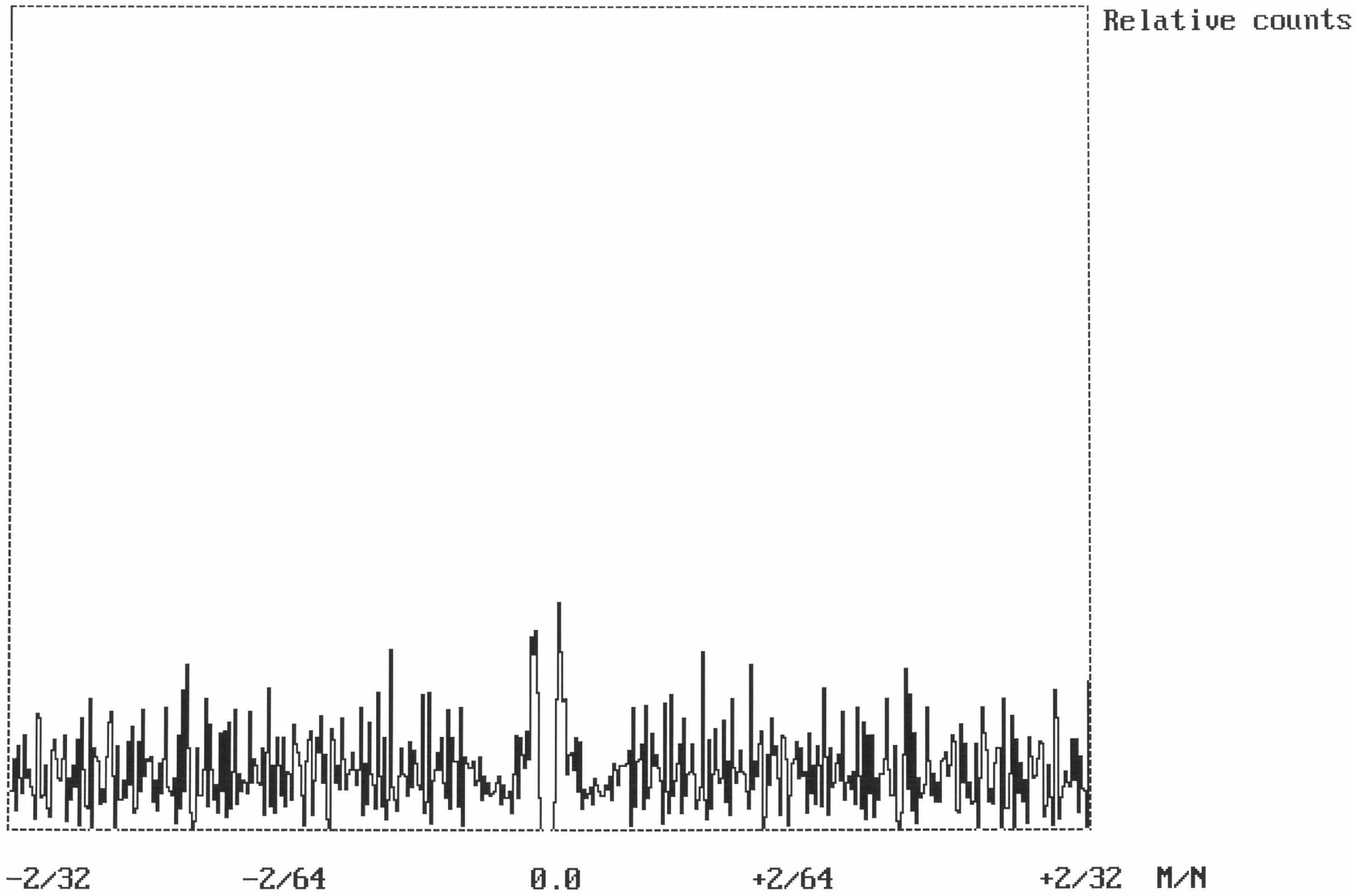

Fig. 43 M/N distribution around M/N=0 with Mod-4 randomizing

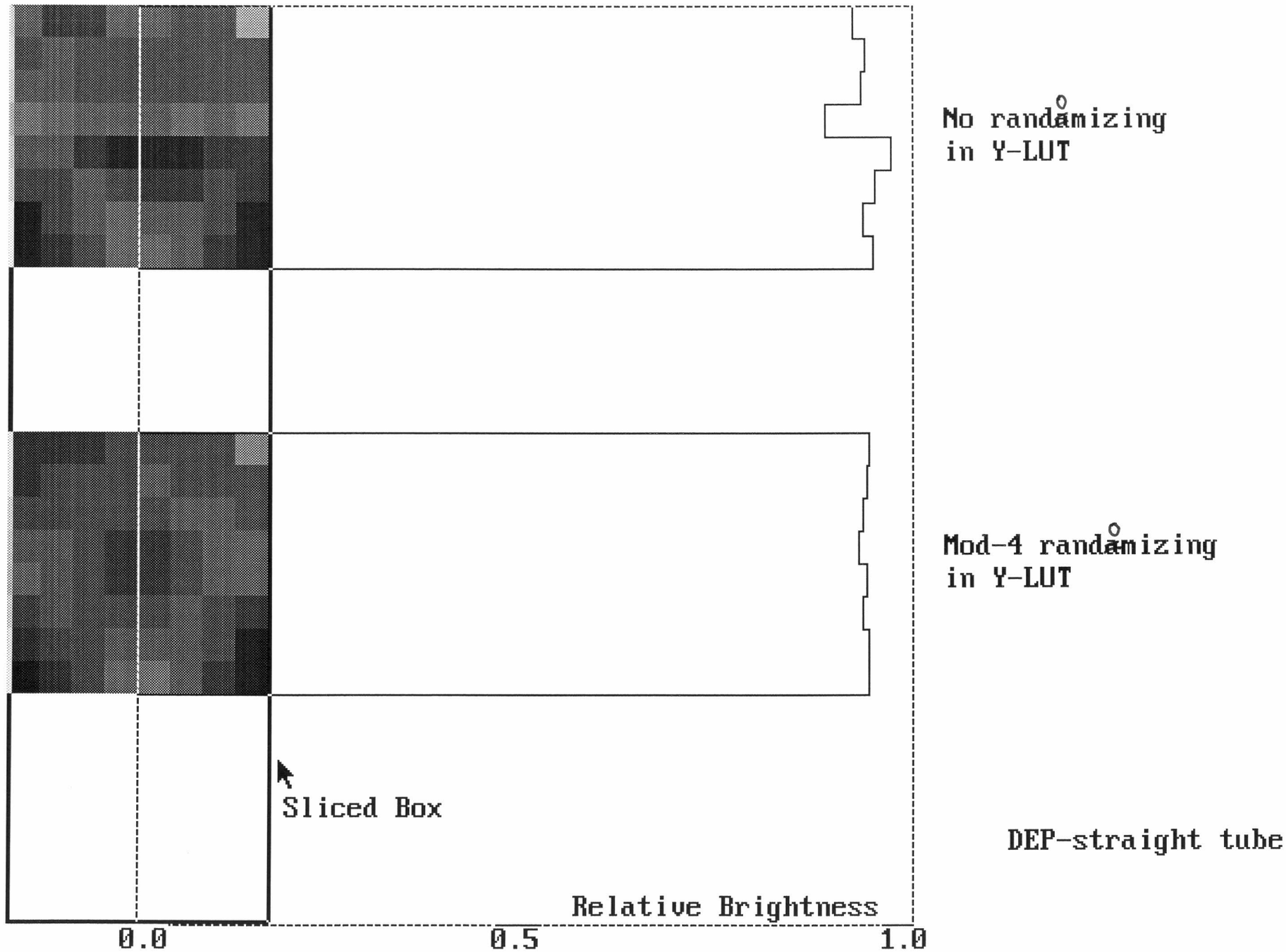

Fig. 44 Fixed pattern caused by the spike at M/N=0

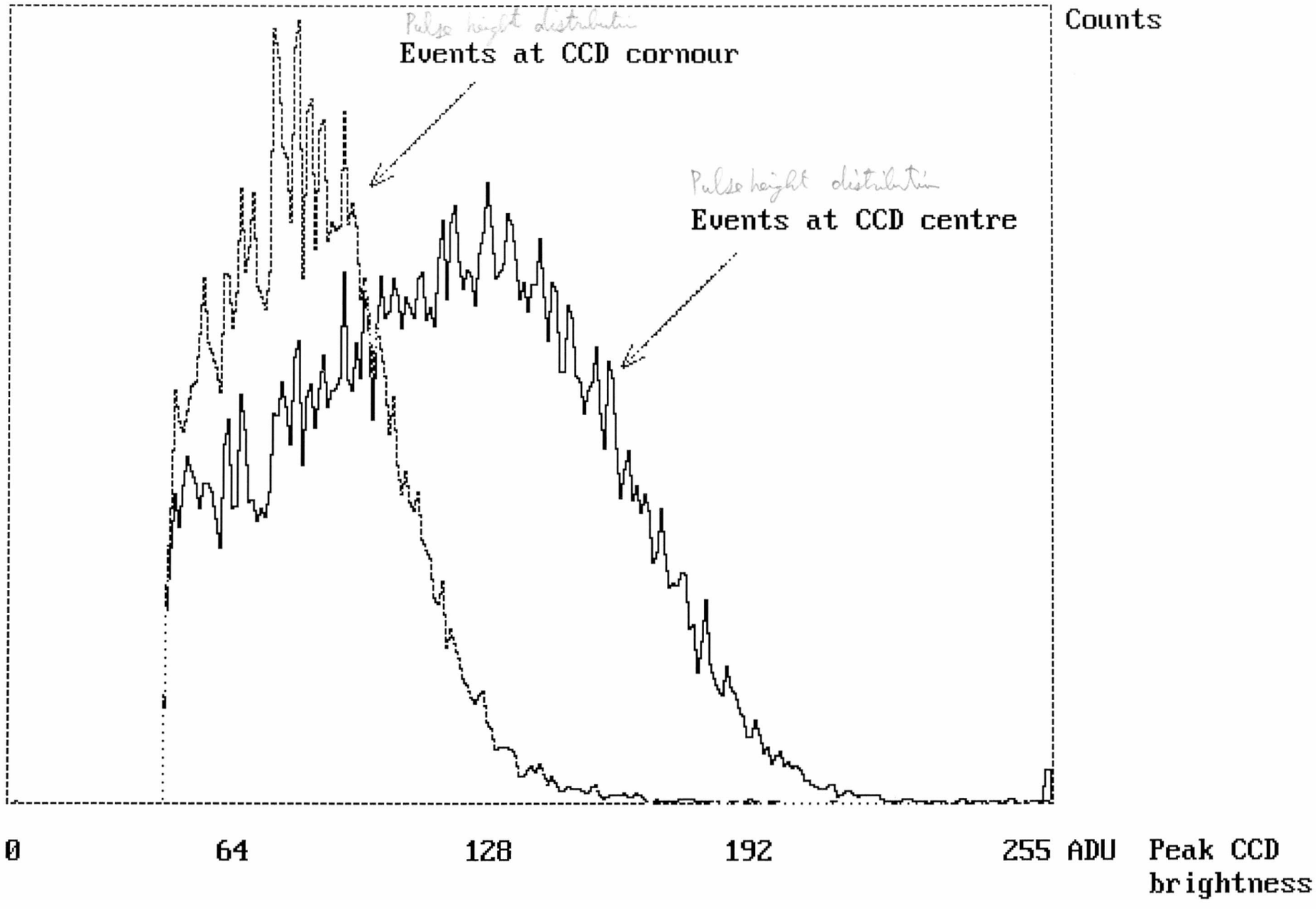

Fig. 45 Variation of brightness at Peak CCD pixel with DEP straight tube